Spinodal decomposition in a binary polymer mixture: Dynamic self-consistent-field theory and Monte Carlo simulations

Ellen Reister, Marcus Müller, and Kurt Binder
Institut für Physik, WA 331, Johannes Gutenberg Universität, D-55099 Mainz, Germany
(Received 30 April 2001; published 25 September 2001)

We investigate how the dynamics of a single chain influences the kinetics of early stage phase separation in a symmetric binary polymer mixture. We consider quenches from the disordered phase into the region of spinodal instability. On a mean field level we approach this problem with two methods: a dynamical extension of the self-consistent-field theory for Gaussian chains, with the density variables evolving in time, and the method of the external potential dynamics where the effective external fields are propagated in time. Different wave vector dependencies of the kinetic coefficient are taken into account. These early stages of spinodal decomposition are also studied through Monte Carlo simulations employing the bond fluctuation model that maps the chains—in our case with 64 effective segments—on a coarse grained lattice. The results obtained through self-consistent-field calculations and Monte Carlo simulations can be compared because the time, length, and temperature scales are mapped onto each other through the diffusion constant, the chain extension, and the energy of mixing. The quantitative comparison of the relaxation rate of the global structure factor shows that a kinetic coefficient according to the Rouse model gives a much better agreement than a local, i.e., wave vector independent, kinetic factor. Including fluctuations in the self-consistent-field calculations leads to a shorter time span of spinodal behavior and a reduction of the relaxation rate for smaller wave vectors and prevents the relaxation rate from becoming negative for larger values of the wave vector. This is also in agreement with the simulation results.

DOI: 10.1103/PhysRevE.64.041804 PACS number(s): 61.25.Hq, 05.10.−a, 64.60.−i, 05.20.Jj

I. INTRODUCTION

Over many years the study of phase transitions in fluid mixtures has become an important field because of their omnipresent occurrence in nature and more importantly because of their technological meaning in creating new materials [1,2]: blending of different species can reduce cost, improve processibility, provide synergy between components, and allow for recycling.

Sophisticated analytical techniques—e.g., self-consistent-field theory [3–6] or polymer reference interaction site model theory [7]—exist for calculating the phase behavior and detailed interfacial properties of polymer blends. Because of the large extension of polymer chains equilibrium properties are well described, however, the analytical description is much less satisfactory for the dynamics of multicomponent systems.

The transition from a completely homogeneous mixture to an equilibrated two phase system is a very long process consisting of a sequence of highly inhomogeneous states. Many different methods to analyze this process have been applied including experiments, theory, and computational simulations. After quenching a polymer blend from the one phase region deep into the two phase region spinodal decomposition takes place. Different time regimes are recognized during spinodal decomposition. During early stages the amplitudes of the concentration fluctuations, that are amplified, are still so small that they do not interact with each other. For later times the local composition reaches the equilibrium value of the coexisting phases, and nonlinear interactions between the fluctuation modes become more and more important. At even later stages hydrodynamics dominates the coarsening [8].

Spinodal decomposition can be approximately described through time dependent Ginzburg-Landau theory, also known as Cahn-Hilliard-Cook theory [9–11]. Many efforts have been made to numerically calculate the time evolution of a mixture in the framework of this theory [12–14]. These calculations are appropriate to give a first insight into how phase separation takes place, but are far from describing the system quantitatively well. Even though binary polymer blends are an ideal testing bed for these approaches, earlier Monte Carlo simulations [15–17] found rather pronounced deviations from their predictions. To find a quantitatively better description, it is necessary to go beyond Ginzburg-Landau theory. Self-consistent-field theory [3–6] (SCFT) has proven to be one of the most successful descriptions of equilibrium properties of polymer mixtures on a mean field level. The idea to use SCFT to develop a dynamical mean field theory is not new [18–21], but, although SCFT describes equilibrium properties well, usually the influence of the single chain dynamics is neglected due to computational expenses, again leading to a more qualitative than quantitative description of the phase separation. In most calculations a simple constant Onsager coefficient is used that would be appropriate if the movement of the polymers were comparable to the movement of point particles. Remembering the connectivity of polymers, it is not likely that this local coupling is sufficient to lead to a quantitatively correct description of the dynamics, and other nonlocal Onsager coefficients have been proposed [22–24].

In this study we are interested in the early stages of spinodal decomposition in an incompressible symmetric binary polymer mixture after a quench from the one phase region to the two phase region paying special attention to the differences in the collective dynamics when the chains obey local

and Rouse dynamics. We therefore employ two dynamical versions of self-consistent-field theory for polymer mixtures. The first method, referred to as dynamic self-consistent-field theory [18,19] (DSCFT), uses the free energy functional of the SCFT for an incompressible mixture in terms of the local composition. This free energy functional leads to a kinetic equation for the time dependent local composition that is integrated numerically. This method has been applied for studying the ordering kinetics in block copolymer and surfactant systems [18,25]. We use both a local and a nonlocal Onsager transport coefficient, as is expected for polymers obeying Rouse dynamics.

The underlying idea of the second method is to express the free energy of the investigated system only in terms of the effective external fields, which are thermodynamically conjugated to the composition. This description leads to an equation of motion for the effective external fields, which is integrated in time. Following Maurits and Fraaije [26] who derived a similar equation of motion neglecting random fluctuations, we refer to this method as the external potential dynamics (EPD), which has been shown to automatically incorporate Rouse dynamics.

The aim of our study is to explore both methods and to investigate the role of the Onsager coefficient. To decide whether our results resemble any ''real'' dynamics a comparison with results obtained through other methods is preferable. Although many experiments have analyzed spinodal decomposition in binary polymer mixtures, only few [27–29] have looked at early stages of demixing and the influence of the Onsager coefficient. Another difficulty in comparing experimental results with our calculations lies in the fact that actual demixing is influenced by many factors, for example, preparation of the probe, polydispersity, or strong dynamic asymmetries due to different glass transition temperatures of the two species [30,31]. Therefore a quantitative mapping between theory and experimental systems is difficult. To gain a quantitative insight we compare our mean field calculations with results obtained through Monte Carlo simulations. No parameters have to be adjusted for this comparison. In the simulations we employ the bond fluctuation model [32,33] that is well established for studying properties of polymer melts. It has been shown that the equilibrium properties of a polymer mixture as given by the self-consistent-field theory are almost quantitatively reproduced through Monte Carlo simulations using the bond fluctuation model [34,35].

Our paper is organized in the following way. In Sec. II we introduce the self-consistent-field theory for a binary polymer mixture, explaining how equilibrium properties can be derived with this method. Then we introduce general aspects of the dynamics in a polymer mixture and show how they can be incorporated in the SCFT leading to dynamic self-consistent-field theory. The following section presents another approach to including dynamics in SCFT regarding the effective external fields as the time dependent variable. Implications regarding density fluctuations in this description are discussed in detail. Section III serves as a brief introduction to the performed Monte Carlo simulations and explains how a direct comparison with SCFT calculations is possible. In Sec. IV, results of our calculations and simulations are presented first showing the difference between the use of local and nonlocal coupling, then comparing the mean field results with the simulations and finally analyzing the influence of random fluctuations. The paper finishes with a summary.

II. SELF-CONSISTENT-FIELD THEORY

We consider an incompressible mixture of A and B polymers consisting of n polymers in a volume $V=L_xL_yL_z$ with periodic boundary conditions. There are n_A polymers of kind A in the system, for B polymers $n_B=n-n_A$. In SCFT [3,5,6,36] polymers are modeled as Gaussian chains with the end-to-end distance R_e. In addition we choose the A and B polymers to both have the same number of monomers $N_A=N_B=N$ and to be of the same architecture. The overall particle density in the system is denoted as $\rho=nN/V$. The microscopic density $\hat{\phi}_A$ of the A monomers can be defined through the polymer conformations $\{\mathbf{r}_\alpha(\tau)\}$,

$$\hat{\phi}_A=\frac{N}{\rho}\sum_{i_A=1}^{n_A}\int_0^1 d\tau\,\delta(\mathbf{r}-\mathbf{r}_{i_A}(\tau)), \tag{1}$$

$0\leqslant\tau\leqslant 1$ parametrizes the contour of a chain. For B monomers a similar equation holds. (All the following equations regarding only A monomers, are equivalently valid for B monomers without mentioning this explicitly.) Regarding a repulsion between the two kinds of polymers that is expressed through the Flory-Huggins parameter χ, the canonical partition function has the following form:

$$Z\sim\frac{1}{n_A!n_B!}\int\left(\prod_{i_A=1}^{n_A}\prod_{i_B=1}^{n_B}\mathcal{D}[\mathbf{r}_{i_A}]\mathcal{D}[\mathbf{r}_{i_B}]\mathcal{P}_A[\mathbf{r}_{i_A}]\mathcal{P}_B[\mathbf{r}_{i_B}]\right)$$
$$\times\exp\left[-\rho\int_V d^3\,\mathbf{r}\chi\hat{\phi}_A\hat{\phi}_B\right]\delta(\hat{\phi}_A+\hat{\phi}_B-1). \tag{2}$$

The functional integral $\mathcal{D}$ sums over all possible conformations of the chains. $\mathcal{P}_A[\mathbf{r}]$ is the so-called Wiener measure

$$\mathcal{P}_A[\mathbf{r}]\sim\exp\left[-\frac{3}{2R_e^2}\int_0^1 d\tau\left(\frac{d\mathbf{r}}{d\tau}\right)^2\right], \tag{3}$$

which represents the statistical weight of a noninteracting Gaussian chain. Repulsive interactions at short interparticle distances reduce fluctuations of the total density. This is incorporated effectively via the incompressibility constraint that is expressed through the δ function in Eq. (2) [37].

This defines a system with many interacting polymer chains; its partition function obviously cannot be analytically solved. Inserting new auxiliary field variables Φ_A, Φ_B, W_A, and W_B via a Hubbard-Stratonovich transformation, we can reformulate the many-polymer problem in terms of a single polymer in external fields.

$$Z \sim \int \mathcal{D}\Phi_A \mathcal{D}W_A \mathcal{D}\Phi_B \mathcal{D}W_B \, \delta(\Phi_A + \Phi_B - 1) \times \exp\{-F[W_A, W_B, \Phi_A, \Phi_B]/k_B T\}. \quad (4)$$

Thus we have found an expression for the canonical free energy depending on the new variables and the single chain partition function Q_A,

$$\frac{F[W_A, W_B, \Phi_A, \Phi_B]}{k_B T} = -\frac{\overline{\phi}_A \rho V}{N} \ln \frac{Q_A}{n_A} - \frac{\overline{\phi}_B \rho V}{N} \ln \frac{Q_B}{n_B} - \frac{\rho}{N} \int_V d^3\mathbf{r} (W_A \Phi_A + W_B \Phi_B) + \frac{\rho}{N} \int_V d^3\mathbf{r} \, \chi N \Phi_A \Phi_B, \quad (5)$$

$\overline{\phi}_A = N n_A / \rho V$ denoting the average density of the A polymers in the system and

$$Q_A = \int \mathcal{D}[\mathbf{r}_A] \mathcal{P}_A[\mathbf{r}] \exp\left[-\int_0^1 d\tau \, W_A(\mathbf{r}(\tau)) \right], \quad (6)$$

being the partition function of a single A chain in the external field W_A.

A. Equilibrium

The functional integral in Eq. (4) also cannot be calculated explicitly. Therefore we employ a saddle point approximation. This means that only the largest contribution to the integrand is considered and the integration does not have to be carried out. The saddle point approximation of Eq. (4) is equivalent to the minimization of the free energy (5) with respect to the auxiliary variables. The values of the fields and densities at the saddle point are denoted by lower case letters and are given by the set of equations that has to be solved self-consistently,

$$\left. \frac{\delta F}{\delta W_A} \right|_{w_A} = 0, \quad \phi_A = -\frac{\overline{\phi}_A V}{Q_A} \frac{\delta Q_A}{\delta w_A} \equiv \phi_A^*[w_A], \quad (7)$$

$$\left. \frac{\delta F}{\delta W_B} \right|_{w_B} = 0, \quad \phi_B = -\frac{\overline{\phi}_B V}{Q_B} \frac{\delta Q_B}{\delta w_B} \equiv \phi_B^*[w_B], \quad (8)$$

$$\left. \frac{\delta F}{\delta \Phi_A} \right|_{\phi_A} - \left. \frac{\delta F}{\delta \Phi_B} \right|_{\phi_B} = 0, \quad w_A - w_B = \chi N (\phi_B - \phi_A), \quad (9)$$

$$\phi_A + \phi_B = 1. \quad (10)$$

The averages of the microscopic densities are given by $\langle \hat{\phi}_A \rangle = \phi_A^*$ and $\langle \hat{\phi}_B \rangle = \phi_B^*$. Equations (7) and (8) make clear that in equilibrium the average microscopic density $\langle \hat{\phi}_A \rangle$ actually equals the thermal average monomer density of a single A chain in an external field w_A. In other words, after starting with a description where we would have to take all possible interactions of every polymer chain into account, see Eq. (2), we have now found a mean field description of the system in which it is sufficient to look at a single chain in an effective external field.

To calculate the monomer densities it is useful to define the end segment distribution $q_A(\mathbf{r},t)$, which gives the probability to find the end of a chain with length t at position $\mathbf{r}$ when exposed to a field w_A,

$$q_A(\mathbf{r},t) = \int \mathcal{D}[\mathbf{r}(t)] \mathcal{P}_A[\mathbf{r}(t)] \delta(\mathbf{r}(t) - \mathbf{r}) \times \exp\left[-\int_0^t d\tau \, w_A(\mathbf{r}(\tau)) \right]. \quad (11)$$

For this end segment distribution the following diffusion equation holds [3]:

$$\frac{\partial q_A(\mathbf{r},t)}{\partial t} = \frac{1}{6} R_e^2 \nabla^2 q_A(\mathbf{r},t) - w_A q_A(\mathbf{r},t), \quad (12)$$

with the boundary condition $q_A(\mathbf{r},0) = 1$. After finding a solution to this equation the monomer density is immediately given through the following expression:

$$\phi_A^*(\mathbf{r}) = \frac{\overline{\phi}_A V}{Q_A} \int_0^1 dt \, q_A(\mathbf{r},t) q_A(\mathbf{r},1-t). \quad (13)$$

The single chain partition function can be calculated with

$$Q_A = \int_V d^3\mathbf{r} \, q_A(\mathbf{r},1). \quad (14)$$

After having presented all necessary equations to calculate equilibrium properties of polymer mixtures, we are now interested in using this description for calculating the dynamics in a polymer mixture. Two ways to achieve this are introduced in the following sections.

B. Dynamic self-consistent-field theory

Because of the fact that the concentrations of the polymers are conserved the continuity equation is valid,

$$\frac{\partial \phi_A(\mathbf{r},t)}{\partial t} + \nabla \cdot \mathbf{J}(\mathbf{r},t) = 0, \quad (15)$$

$\mathbf{J}(\mathbf{r},t)$ denoting the current density of the monomers at position $\mathbf{r}$ at time t. One now assumes [22–24] a linear relation between the current density and the gradient of the exchange potential $\mu = \delta F/(\delta \phi_A) - \delta F/(\delta \phi_B)$ (note that there is only one independent chemical potential in the system because of the incompressibility constraint),

$$\mathbf{J}(\mathbf{r},t) = -\int_V d\mathbf{r}'^3 \Lambda(\mathbf{r},\mathbf{r}') \nabla \mu(\mathbf{r}',t), \quad (16)$$

with the kinetic coefficient $\Lambda(\mathbf{r},\mathbf{r}')$ describing the connection between the force acting on the monomers through the gradient of the chemical potential at position $\mathbf{r}'$ and the re-

sulting current density at position $\mathbf{r}$. This describes a purely relaxational dynamics, effects due to hydrodynamic flow are not captured. The Onsager coefficient Λ can be modeled in different ways. The simplest approach would be local coupling that results in the Onsager coefficient being proportional to the local density. Bearing in mind that polymers have a certain extension it is clear that nonlocal coupling should lead to a better description, although local coupling is often used in calculations of dynamic models based on Ginzburg-Landau type energy functionals for simplicity reasons [12–14]. In the Rouse model, forces acting on a monomer caused by the other monomers are also taken into account [38,39]. This leads to a kinetic factor that is proportional to the pair-correlation function [22–24,26]. These two approaches lead to the following Onsager coefficients:

$$\Lambda_{\mathrm{local}}(\mathbf{r}) = DN\phi_A(\mathbf{r},t)\,\phi_B(\mathbf{r},t) \quad \text{(local coupling)}, \tag{17}$$

$$\Lambda_{\mathrm{Rouse}}(\mathbf{r},\mathbf{r}') \approx DN\overline{\phi}_A\overline{\phi}_B P_0(\mathbf{r},\mathbf{r}') \quad \text{(Rouse)}, \tag{18}$$

D denoting the single chain diffusion constant and $P_0(\mathbf{r},\mathbf{r}')$ the pair-correlation function. The Rouse Onsager coefficient written in Eq. (18) is only approximately valid, when the pair-correlation function is the same for both polymer species. A more general expression is found in Ref. [26].

Another model for nonlocal coupling is the reptation model [39,40] that is appropriate for polymer melts with very long chains, i.e., very entangled chains. Hereby the idea is that a polymer chain is constrained by the other polymers and is forced to move along the polymer tube axis. This dynamics is expected [22–24] to also lead to an Onsager coefficient that is proportional to the pair-correlation function. Therefore the influence of single chain Rouse and reptation dynamics on the collective dynamics of the system is qualitatively comparable. Reptation shall not be regarded in the further study.

Equations (15) and (16) lead to the following diffusion equation, the last term representing noise that obeys the fluctuation-dissipation theorem,

$$\frac{\partial\phi_A(\mathbf{r},t)}{\partial t} = \boldsymbol{\nabla}\cdot\int_V d\mathbf{r}'^3\Lambda(\mathbf{r},\mathbf{r}')\boldsymbol{\nabla}\mu(\mathbf{r}',t) + \eta(\mathbf{r},t). \tag{19}$$

After the Fourier transformation this diffusion equation has a simple form,

$$\frac{\partial\phi_A(\mathbf{q},t)}{\partial t} = -\Lambda(\mathbf{q})q^2\mu(\mathbf{q},t) + \eta(\mathbf{q},t). \tag{20}$$

These diffusion equations implicitly assume that the relaxation time of the chain conformations is smaller than the time scale on which composition fluctuations evolve. The chain conformations are expected to be ''in equilibrium'' with respect to the instantaneous spatially varying composition.

To use the introduced diffusion equation (19) in the frame of SCFT, let us return to the general expression (4) that describes the canonical partition function depending upon the variables Φ_A, Φ_B, W_A, and W_B that are independent of each other. If we now employ a saddle point approximation in the variables W_A and W_B we find Eqs. (7) and (8) that describe a unique relation between the fields w_A and w_B and the densities ϕ_A and ϕ_B. This means we can calculate the densities explicitly with Eqs. (12), (13), and (14) if the fields w_A and w_B are known. Therefore with this approximation the free energy F becomes a function that depends on the densities (or fields) only: $F[\phi_A,\phi_B,w_A[\phi_A],w_B[\phi_B]] = F[\phi_A,\phi_B]$. With this free energy it is now possible to calculate the exchange potential $\mu(\mathbf{r})$,

$$\begin{aligned}\frac{\mu(\mathbf{r})}{k_BT} &= \frac{\delta F[\phi_A(\mathbf{r}),\phi_B(\mathbf{r})]}{\delta\phi_A(\mathbf{r})} - \frac{\delta F[\phi_A(\mathbf{r}),\phi_B(\mathbf{r})]}{\delta\phi_B(\mathbf{r})} \\ &= \frac{1}{N}\{\chi N[\phi_B(\mathbf{r})-\phi_A(\mathbf{r})] \\ &\quad -(w_A[\phi_A(\mathbf{r})]-w_B[\phi_B(\mathbf{r})])\}.\end{aligned} \tag{21}$$

The simple form of diffusion equation (20) and the diffusion equation for the end segment distribution of a polymer chain, Eq. (12), suggests the use of a Fourier expansion of all spatially dependent variables for actual calculations because the Fourier functions are eigenfunctions of the squared gradient $\boldsymbol{\nabla}^2$. The following set of orthonormal functions is used in all our SCFT calculations:

$$\begin{aligned}f_{lmn}(\mathbf{r}) &= \mathrm{norm}(l)\,\mathrm{norm}(m)\,\mathrm{norm}(n) \\ &\quad\times\cos\left(\frac{2\pi l}{L_x}x\right)\cos\left(\frac{2\pi m}{L_y}y\right)\cos\left(\frac{2\pi n}{L_z}z\right) \\ l,m,n &= 0,1,2,\ldots, \\ \mathrm{norm}(i) &= \begin{cases}\sqrt{2}, & i\neq 0\\ 1, & i=0.\end{cases}\end{aligned} \tag{22}$$

We have now found all necessary equations to numerically calculate the time evolution of the densities in a binary polymer mixture, leading us to the following procedure we refer to as the DSCFT method. First we have a given density profile at time $t=0$. As mentioned before, Eqs. (12), (13), and (14) give us the possibility to explicitly calculate the single chain densities for known external fields. Unfortunately the inversion is needed because we have given densities and have to find the matching external fields. This leads to a set of nonlinear equations that are numerically solved through the Newton-Broyden method [41]. After the external fields, which ''create'' the given density profile, have been found the exchange potential μ is calculated via Eq. (21) and then inserted into the diffusion equation (20). The diffusion equation is subsequently integrated using a simplified Runge-Kutta method. This leads to a new given density after a discrete time step and the whole procedure starts anew.

Apart from regarding local dynamics in our DSCFT calculations it is favorable to consider nonlocal coupling because this leads to a better description of the dynamics in a polymer mixture. However, in DSCFT the difficulty in using Rouse dynamics lies in the computational expense of calculating the pair-correlation function for each time step. As an approximation during early stages of demixing the pair-correlation function of a homogeneous melt, as it is given through the random phase approximation (RPA) [42], is used leading to the following Onsager coefficient:

$$\Lambda(q)=DN\overline{\phi}_A\overline{\phi}_B\frac{2(x+e^{-x}-1)}{x^2}, \tag{23}$$

x is defined as $x=R_e^2\mathbf{q}^2/6$ with R_e denoting the end-to-end distance of a polymer.

C. External potential dynamics

In the previously introduced DSCFT method we needed a way to reduce the number of independent variables in the partition function. Through the saddle point approximation in the fields we obtained a free energy functional in terms of the densities. This, in turn, yields a Langevin equation for the dynamics of the densities. For the EPD method [26] we are looking for a way to express the dynamics of the binary polymer mixture through an equation of motion for the external fields W_A and W_B. Our starting point is again the canonical partition function (2). Via a Hubbard-Stratonovich transformation we introduce the field variables $W=W_A-W_B$ and $U=W_A+W_B$ and obtain

$$\begin{aligned}
Z\sim&\frac{1}{n_A!n_B!}\int\left(\prod_{i_A=1}^{n_A}\prod_{i_B=1}^{n_B}\mathcal{D}[\mathbf{r}_{i_A}]\mathcal{D}[\mathbf{r}_{i_B}]\mathcal{P}_A[\mathbf{r}_{i_A}]\mathcal{P}_B[\mathbf{r}_{i_B}]\right)\\
&\times\exp\left[-\rho\int_V d^3\mathbf{r}\frac{\chi}{4}\{(\hat{\phi}_A+\hat{\phi}_B)^2-(\hat{\phi}_A-\hat{\phi}_B)^2\}\right]\\
&\times\delta(\hat{\phi}_A+\hat{\phi}_B-1)\\
\sim&\frac{1}{n_A!n_B!}\int\left(\prod_{i_A=1}^{n_A}\prod_{i_B=1}^{n_B}\mathcal{D}[\mathbf{r}_{i_A}]\mathcal{D}[\mathbf{r}_{i_B}]\mathcal{P}_A[\mathbf{r}_{i_A}]\mathcal{P}_B[\mathbf{r}_{i_B}]\right)\\
&\times\int\mathcal{D}U\mathcal{D}W\exp\left[-\frac{\rho V\chi}{4}\right]\exp\left[-\frac{\rho}{N}\int_V d^3\mathbf{r}\left\{\frac{W}{2}(\hat{\phi}_A-\hat{\phi}_B)\right.\right.\\
&\left.\left.+\frac{W^2}{4\chi N}\right\}\right]\exp\left[-\frac{\rho}{N}\int_V d^3\mathbf{r}\ \frac{U}{2}(\hat{\phi}_A+\hat{\phi}_B-1)\right].
\end{aligned}\tag{24}$$

This defines a free energy function G in terms of the fields U and W,

$$\mathcal{Z}\sim\int\mathcal{D}U\mathcal{D}W\exp(-G[U,W]/k_BT), \tag{25}$$

with

$$\begin{aligned}
\frac{G[U,W]}{k_BT}=&-\frac{\overline{\phi}_A\rho V}{N}\ln\frac{Q_A[(U+W)/2]}{n_A}\\
&-\frac{\overline{\phi}_B\rho V}{N}\ln\frac{Q_B[(U-W)/2]}{n_B}\\
&+\frac{\rho}{N}\int_V d^3\mathbf{r}\left[\frac{W^2}{4\chi N}-\frac{1}{2}\left(U-\frac{\chi N}{2}\right)\right].
\end{aligned}\tag{26}$$

Alternatively, we could have started with the free energy functional (4) and integrate out the Gaussian variables Φ_A and Φ_B. So far no approximations have been used, but to find an energy functional that only depends upon W we now employ a saddle point approximation with respect to U,

$$\frac{\delta G[U,W]}{\delta U}|_{U*}=0,\quad \phi_A^*(\mathbf{r})+\phi_B^*(\mathbf{r})=1. \tag{27}$$

Here we use the definition, see Eqs. (7) and (8), $\phi_A^*=-(\overline{\phi}_AV/Q_A)(\delta Q_A/\delta W_A)$. For ϕ_B^* the equivalent definition applies. In equilibrium the field variable $U=W_A+W_B$ is conjugated to the overall density of the system, which is constant in an incompressible mixture. We therefore believe that the influence of this approximation on the description of the system through the field W is very small. We shall discuss this in detail below.

If we replace U with the $U^*[W]$ that fulfils this constraint we end up with a free energy functional that only depends on the field variable W,

$$\begin{aligned}
\frac{G[W(\mathbf{r})]}{k_BT}=&\frac{\rho V\chi}{4}+\frac{\rho}{N}\int_V d^3\mathbf{r}\frac{W^2}{4\chi N}\\
&-\frac{\overline{\phi}_A\rho V}{N}\ln\frac{Q_A[(U^*+W)/2]}{n_A}\\
&-\frac{\overline{\phi}_B\rho V}{N}\ln\frac{Q_B[(U^*-W)/2]}{n_B},
\end{aligned}\tag{28}$$

where we have used the fact that adding a constant field ξ to U^* does not change the value of $G[W(\mathbf{r})]$. We chose ξ in such a way that $\int_V d^3\mathbf{r}\ U^*=0$.

A difficulty in describing the system with the order parameter W is the interpretation of the field fluctuations in terms of the physical density fluctuations. We can calculate the averages of the microscopic densities *after* the saddle point integration over U. These averages are marked by the

subscript EPD. To this end, we introduce a local exchange potential $\Delta\mu$, which couples to the microscopic density difference $\hat{\phi}_A-\hat{\phi}_B$,

$$\begin{aligned}\tilde{\mathcal{Z}}[\Delta\mu]\sim&\frac{1}{n_A!n_B!}\int\left(\prod_{i_A=1}^{n_A}\prod_{i_B=1}^{n_B}\mathcal{D}[\mathbf{r}_{i_A}]\mathcal{D}[\mathbf{r}_{i_B}]\right.\\&\left.\times\mathcal{P}_A[\mathbf{r}_{i_A}]\mathcal{P}_B[\mathbf{r}_{i_B}]\right)\\&\times\exp\left[-\frac{\rho}{N}\int_V d^3\mathbf{r}\left\{\frac{\Delta\mu}{2}(\hat{\phi}_A-\hat{\phi}_B)\right\}\right]\\&\times\int\mathcal{D}W\exp\left[-\frac{\rho V\chi}{4}\right]\\&\times\exp\left[-\frac{\rho}{N}\int_V d^3\mathbf{r}\left\{\frac{W}{2}(\hat{\phi}_A-\hat{\phi}_B)+\frac{W^2}{4\chi N}\right\}\right]\\&\times\exp\left[-\frac{\rho}{N}\int_V d^3\mathbf{r}\ \frac{U^*[W]}{2}(\hat{\phi}_A+\hat{\phi}_B-1)\right]\\\sim&\int\mathcal{D}W\exp(-\tilde{G}[W,\Delta\mu]),\end{aligned}$$

with

$$\begin{aligned}\tilde{G}[W,\Delta\mu]=&\frac{\rho V\chi}{4}+\frac{\rho}{N}\int_V d^3\mathbf{r}\ \frac{W^2}{4\chi N}\\&-\frac{\overline{\phi}_A\rho V}{N}\ln\frac{Q_A[(U^*+W+\Delta\mu)/2]}{n_A}\\&-\frac{\overline{\phi}_B\rho V}{N}\ln\frac{Q_B[(U^*-W-\Delta\mu)/2]}{n_B}.\end{aligned}\tag{29}$$

Thermodynamic averages of the microscopic density difference are obtained via functional derivatives,

$$\begin{aligned}\langle\hat{\phi}_A(\mathbf{r})-\hat{\phi}_B(\mathbf{r})\rangle_{\mathrm{EPD}}=&-\frac{2N}{\rho}\frac{1}{\tilde{\mathcal{Z}}[\Delta\mu]}\frac{\delta\tilde{\mathcal{Z}}[\Delta\mu]}{\delta\Delta\mu(\mathbf{r})}\bigg|_{\Delta\mu=0}\\=&\langle\phi_A^*(\mathbf{r})-\phi_B^*(\mathbf{r})\rangle\end{aligned}\tag{30}$$

$$\begin{aligned}&\langle[\hat{\phi}_A(\mathbf{r})-\hat{\phi}_B(\mathbf{r})][\hat{\phi}_A(\mathbf{r}')-\hat{\phi}_B(\mathbf{r}')]\rangle_{\mathrm{EPD}}\\&=\left(\frac{2N}{\rho}\right)^2\frac{1}{\tilde{\mathcal{Z}}[\Delta\mu]}\frac{\delta^2\tilde{\mathcal{Z}}[\Delta\mu]}{\delta\Delta\mu(\mathbf{r})\delta\Delta\mu(\mathbf{r}')}\bigg|_{\Delta\mu=0}\\&=\langle[\phi_A^*(\mathbf{r})-\phi_B^*(\mathbf{r})][\phi_A^*(\mathbf{r}')-\phi_B^*(\mathbf{r}')]\rangle\\&\quad-\frac{N}{\rho}\left\langle\frac{\delta\phi_A^*(\mathbf{r})}{\delta W_A(\mathbf{r}')}+\frac{\delta\phi_B^*(\mathbf{r})}{\delta W_B(\mathbf{r}')}\right\rangle.\end{aligned}\tag{31}$$

Similarly, we can calculate the fluctuations of the total density, which are induced by the saddle point approximation.

$$\begin{aligned}\tilde{\mathcal{Z}}[\mu]\sim&\frac{1}{n_A!n_B!}\int\left(\prod_{i_A=1}^{n_A}\prod_{i_B=1}^{n_B}\mathcal{D}[\mathbf{r}_{i_A}]\mathcal{D}[\mathbf{r}_{i_B}]\mathcal{P}_A[\mathbf{r}_{i_A}]\mathcal{P}_B[\mathbf{r}_{i_B}]\right)\\&\times\exp\left[-\frac{\rho}{N}\int_V d^3\mathbf{r}\left\{\frac{\mu}{2}(\hat{\phi}_A+\hat{\phi}_B)\right\}\right]\\&\times\int\mathcal{D}W\exp\left[-\frac{\rho V\chi}{4}\right]\\&\times\exp\left[-\frac{\rho}{N}\int_V d^3\mathbf{r}\left\{\frac{W}{2}(\hat{\phi}_A-\hat{\phi}_B)+\frac{W^2}{4\chi N}\right\}\right]\\&\times\exp\left[-\frac{\rho}{N}\int_V d^3\mathbf{r}\ \frac{U^*[W]}{2}(\hat{\phi}_A+\hat{\phi}_B-1)\right]\\\sim&\int\mathcal{D}W\exp(-\tilde{G}[W,\mu])\end{aligned}$$

with

$$\begin{aligned}\tilde{G}[W,\mu]=&\frac{\rho V\chi}{4}+\frac{\rho}{N}\int_V d^3\mathbf{r}\ \frac{W^2}{4\chi N}\\&-\frac{\overline{\phi}_A\rho V}{N_A}\ln\frac{Q_A[(U^*+W+\mu)/2]}{n_A}\\&-\frac{\overline{\phi}_B\rho V}{N_B}\ln\frac{Q_B[(U^*-W+\mu)/2]}{n_B}.\end{aligned}\tag{32}$$

Moments of the total density averaged over the field configurations of W are given by

$$\begin{aligned}&-\frac{\rho}{2N}\langle\hat{\phi}_A(\mathbf{r})+\hat{\phi}_B(\mathbf{r})\rangle_{\mathrm{EPD}}\\&=\frac{1}{\tilde{\mathcal{Z}}[\mu]}\frac{\delta\tilde{\mathcal{Z}}[\mu]}{\delta\mu(\mathbf{r})}\bigg|_{\mu=0},\\&\Rightarrow\langle\hat{\phi}_A(\mathbf{r})+\hat{\phi}_B(\mathbf{r})\rangle_{\mathrm{EPD}}=\langle\phi_A^*(\mathbf{r})+\phi_B^*(\mathbf{r})\rangle=1,\end{aligned}\tag{33}$$

$$\begin{aligned}&\left(\frac{\rho}{2N}\right)^2\langle[\hat{\phi}_A(\mathbf{r})+\hat{\phi}_B(\mathbf{r})][\hat{\phi}_A(\mathbf{r}')+\hat{\phi}_B(\mathbf{r}')]\rangle_{\mathrm{EPD}}\\&=\frac{1}{\tilde{\mathcal{Z}}[\mu]}\frac{\delta^2\tilde{\mathcal{Z}}[\mu]}{\delta\mu(\mathbf{r})\delta\mu(\mathbf{r}')}\bigg|_{\mu=0},\\&\Rightarrow\langle[\hat{\phi}_A(\mathbf{r})+\hat{\phi}_B(\mathbf{r})][\hat{\phi}_A(\mathbf{r}')+\hat{\phi}_B(\mathbf{r}')]\rangle_{\mathrm{EPD}}\\&=1-\frac{N}{\rho}\left\langle\frac{\delta\phi_A^*(\mathbf{r})}{\delta W_A(\mathbf{r}')}+\frac{\delta\phi_B^*(\mathbf{r})}{\delta W_B(\mathbf{r}')}\right\rangle.\end{aligned}\tag{34}$$

These equations describe the actual fluctuations of the microscopic composition of the system *after* the saddle point approximation, i.e., of the EPD method. Having performed a saddle point integration in U, we have ignored fluctuations,

and we cannot expect Eqs. (31) or (34) to be accurate. Indeed, while the incompressibility constraint is fulfilled *on average* Eq. (34) demonstrates that the saddle point approximation leads to spurious fluctuations of the total density. In Appendix B we use RPA to evaluate Eq. (31) and show explicitly the deviations between Eq. (31) and the well known RPA-structure factor.

Alternatively, we can deduce the exact averages from the full free energy functional $G[U,W]$ in Eq. (26) by introducing a local exchange potential $\Delta\mu$ like in Eq. (29). After a variable substitution $W+\Delta\mu\rightarrow W$ this leads to

$$\tilde{G}[U,W,\Delta\mu]=G[U,W]-\frac{\rho}{N}\int_V d^3\mathbf{r}\ \frac{-\Delta\mu^2+2\Delta\mu W}{4\chi N}. \tag{35}$$

With this free energy functional we obtain the exact averages of the microscopic densities,

$$\langle\hat{\phi}_A(\mathbf{r})-\hat{\phi}_B(\mathbf{r})\rangle_{UW}=-\frac{1}{\chi N}\langle W\rangle_{UW}, \tag{36}$$

$$\langle[\hat{\phi}_A(\mathbf{r})-\hat{\phi}_B(\mathbf{r})][\hat{\phi}_A(\mathbf{r}')-\hat{\phi}_B(\mathbf{r}')]\rangle_{UW} =\frac{-2\delta(\mathbf{r}-\mathbf{r}')}{\rho\chi}+\frac{1}{(\chi N)^2}\langle W(\mathbf{r})W(\mathbf{r}')\rangle_{UW}. \tag{37}$$

Recently, Ganesan and Fredrickson [43] have used a complex Langevin method to sample the fluctuations of both fields U and W, and have obtained the average A-monomer density as $\langle\phi_A^*\rangle_{UW}$. Since U has to be complex to make the last term in Eq. (24) a proper representation of $\delta(\hat{\phi}_A+\hat{\phi}_B-1)$ individual contributions to this average also have an imaginary part and the numerical procedure is quite involved.

We expect the saddle point integration over U to be accurate whenever $G[U,W]$ can be well approximated by a parabola in $U-U^*$. In this case the fluctuations of W are only very little affected by the saddle point approximation in U and the fluctuations of W in the EPD method will closely mimic the fluctuations of W of the exact partition function (24). Hence, we can use Eq. (37) with $\langle W(\mathbf{r})W(\mathbf{r}')\rangle_{UW}\approx\langle W(\mathbf{r})W(\mathbf{r}')\rangle$ (i.e., *after* the saddle point approximation) to obtain a very good approximation for the structure factor. In Appendix B we confirm that in RPA the fluctuations of W are, of course, not affected by the saddle point integration over U. Therefore we use the Fourier transform of Eqs. (36) and (37) in our calculations,

$$\langle\phi_A(q)-\phi_B(q)\rangle=-\frac{1}{\chi N}\langle W(q)\rangle, \tag{38}$$

$$\langle|\phi_A(q)-\phi_B(q)|^2\rangle=-\frac{2}{\rho V\chi}+\frac{1}{(\chi N)^2}\langle|W(q)|^2\rangle. \tag{39}$$

Because the composition is conserved and $\langle\hat{\phi}_A-\hat{\phi}_B\rangle\sim\langle W\rangle$, we expect the order parameter W with which we are now describing our system to also be a conserved quantity. Therefore the dynamics of W are given through the relaxational dynamics of a model B system, referring to the classification introduced by Hohenberg and Halperin [44].

$$\frac{\partial W(\mathbf{r})}{\partial t}=\nabla_{\mathbf{r}}\cdot\int_V\Lambda(\mathbf{r},\mathbf{r}')\nabla_{\mathbf{r}'}\mu_W(\mathbf{r}')+\eta(\mathbf{r},t), \tag{40}$$

with the chemical potential being the first derivative of the free energy with respect to the order parameter,

$$\mu_W(\mathbf{r})=\frac{\delta G[W(\mathbf{r})]}{\delta W(\mathbf{r})}=\frac{1}{N2\chi N}\{W+\chi N[\phi_A^*(\mathbf{r})-\phi_B^*(\mathbf{r})]\}. \tag{41}$$

The Fourier transform of this new diffusion equation is

$$\frac{\partial W(q)}{\partial t}=-\Lambda(q)q^2\frac{1}{2N\chi N}\{W(q)+\chi N[\phi_A^*(q)-\phi_B^*(q)]\}+\eta(q), \tag{42}$$

η is white noise that obeys the fluctuation-dissipation theorem. The method using this diffusion equation we refer to as the EPD method [26].

We have found a diffusion equation that describes the dynamics in terms of the external field $W=W_A-W_B$ and leads to the right physical equilibrium. A similar equation without noise has been derived by Maurits and Fraaije [26]. The question to be asked is whether this dynamics represents any actual physical dynamics and how the choice of the Onsager coefficient influences the dynamics of the densities. It can be shown [26], see also appendix A, that using local coupling in the EPD method is a good approximation for Rouse dynamics. The Onsager coefficient that we would have to use in DSCFT to reproduce Rouse dynamics is given in Eq. (18). The equivalent (local) kinetic coefficient in the EPD method for the same dynamics of the densities is

$$\Lambda_{\mathrm{EPD}}=-2\chi ND. \tag{43}$$

For the EPD calculations again the Fourier expansion of Eq. (22) is used. After having found the initial fields that create the given densities with the methods used for the DSCFT, the chemical potential μ_W is calculated according to Eq. (41). μ_W is then plugged into Eq. (42) to find the time derivative of the difference in the fields. Thereafter $\partial W/\partial t=\partial W_A/\partial t-\partial W_B/\partial t$ is integrated via the simplified Runge-Kutta method. After we have found the new $W=W_A-W_B$, we need to find the variable U^* to make sure the incompressibility constraint $\phi_A^*+\phi_B^*=1$ given through the saddle point approximation (27) is fulfilled again using the Newton-Broyden method. The new fields lead us to the new chemical potential to calculate $\partial W/\partial t=\partial W_A/\partial t-\partial W_B/\partial t$ and so forth.

The method of the EPD has two main advantages compared to DSCFT. First of all it incorporates nonlocal coupling, and second, it proves to be up to an order of magni-

tude computationally faster. There are two main reasons for this huge speed up: In EPD the number of equations that have to be solved via the Newton-Broyden method to fulfil incompressibility is just the number of Fourier functions used. The number of equations in DSCFT that have to be solved to find the new fields after integrating the densities is twice as large. On the other hand, comparing diffusion equation (19) used in the DSCFT method with Eq. (40) in EPD, it is easily seen that the right-hand side of the latter is a simple multiplication with the squared wave vector of the relevant mode, whereas the right-hand side of Eq. (19) is a complicated multiplication of three spatially dependent variables.

III. MONTE CARLO SIMULATIONS

A. Bond fluctuation model

The Monte Carlo simulations presented in this study make use of the bond fluctuation model [32,33], which is a coarse grained lattice model, that incorporates the relevant features of polymers. These are connectivity of the monomers along a chain, excluded volume of the segments, and thermal interaction between monomers. In this model each effective monomer occupies a cube of the lattice and blocks the eight sites at the cube corners for other monomers. Monomers of a chain are connected by one of 108 possible bond vectors of length 2, $\sqrt{5}$, $\sqrt{6}$, 3, or $\sqrt{10}$ measured in units of the lattice spacing. (All following lengths are assumed to be given in these units unless an explicit unit is given.) These bond vectors are chosen to ensure the excluded volume condition, which makes sure that they do not cross each other during their movement. This large number of possible bond vectors allows 87 different bond angles, which provide a good approximation for continuous connectivity between the monomers of the chain. Each of the effective monomers represents three to five real chemical repeat units [45,46]. The number density of the occupied sites is chosen to be $\rho=1/16$, which reproduces the properties of a polymer melt well. Interactions between the monomers are modeled through a square well potential with monomers of the same kind attracting and monomers of different kinds repelling each other. The interactions are chosen to be symmetric and to act inside a radius that extends over the first peak of the pair correlation function. This means the interactions act up to a distance of $\sqrt{6}$ that is equivalent to the 54 neighboring cubes of a monomer.

$$-\epsilon_{AA}=-\epsilon_{BB}=\epsilon_{AB}=\begin{cases} k_BT\epsilon\geqslant 0, & \text{for } r\leqslant\sqrt{6} \\ 0, & \text{for } r>\sqrt{6}. \end{cases} \tag{44}$$

The moves used to simulate a purely diffusive movement of the monomers are local random monomer hopping moves, where one tries to move a randomly picked monomer to a neighboring lattice site.

B. Comparison between SCFT calculations and Monte Carlo simulations

The Monte Carlo simulations were carried out with chains of 64 effective segments in a box with length $L=160$. With an overall number density of $\rho=1/16$ there are 256 000 particles in the system. In the Monte Carlo simulations, however, the choice of $N=64$, which is equivalent to a polymerization of 200–300 in real polymers, is a compromise between the possibility to compare the simulation results with mean field results and the largest still sensibly manageable amount of computational resources, because an increase in the polymerization leads to both an increase in the length scale and a slowing down in the kinetics of phase separation. To actually compare Monte Carlo simulations with SCFT calculations the parameters of both models have to mapped onto each other.

In SCFT the only present length scale is the end-to-end distance R_e of the polymers. It can be measured directly in the Monte Carlo simulations $R_e=\sqrt{N}b=25.12$. This gives us the length of the system to be $L=160=6.35R_e$.

In the SCFT calculations, only the combination χN of the Flory Huggins parameter and chain length enters. This sets the temperature scale. The Flory Huggins parameter χ can be calculated from the interaction parameter ϵ of the square well potential defining the interaction between monomers in the Monte Carlo simulations with the following relation [47]:

$$\chi=\frac{1}{k_BT}z_{\text{eff}}\left[\epsilon_{AB}-\frac{1}{2}(\epsilon_{AA}+\epsilon_{BB})\right]=2z_{\text{eff}}\epsilon, \tag{45}$$

z_{eff} is the effective coordination number in the bulk, i.e., the average number of intermolecular contacts per monomer. We hereby speak of contacts, if the distance between the monomers is smaller than $\sqrt{6}$.

The average composition $\overline{\phi_A}$ is a parameter of the SCFT, the total number density ρ of monomers is only required if fluctuations are considered.

The single chain diffusion constant D, which can be extracted from the Monte Carlo simulations by measuring the mean square displacements of the chains, gives the time scale $\tau=R_e^2/D=1.5\times10^7$ Monte Carlo steps (MCS). τ is constant because D and R_e are almost independent of time and composition [48].

The length of the chains used in the Monte Carlo simulations is $N=64$. This is somewhat larger than the entanglement length $N_e\approx32$ [45,46], therefore, we are in a crossover regime between Rouse dynamics and reptation [49,50]. This means, when we are comparing dynamic mean field results with Monte Carlo results we expect to find a reasonable agreement if we regard Rouse dynamics.

This identifies all parameters of the SCFT calculations (without noise). If we neglect fluctuations, systems with identical χN, R_e, and composition but different degree of interdigitation $\rho R_e^3/N$ [34,51] and statistical segment length $b=R_e^2/N$ give identical results. The degree of interdigitation controls the strength of fluctuations and mean field theory is believed to be correct in the limit $\rho R_e^3/N\rightarrow\infty$. The statistical segment length sets the smallest length scale for which the Gaussian description of polymers is valid. If we were interested in the structure on smaller length scales we would have to use a different chain model (e.g., wormlike chain [52,53]).

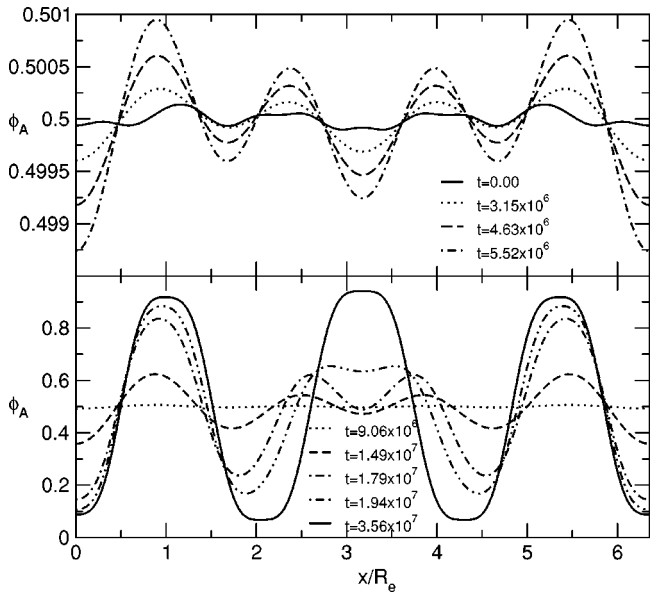

FIG. 1. Density profiles at different times during demixing after a quench from $\chi N=0.314$ to $\chi N=5$ in a one-dimensional system using 12 eigenfunctions. The upper panel shows the early stages when concentration fluctuations with wavelengths between one-third and one-fourth of the system size are amplified. In the lower panel later stages are displayed–the concentration inside a domain slowly saturates leading to sharp interfaces between the coexisting phases. Note the change of scale on the composition axis between the two panels.

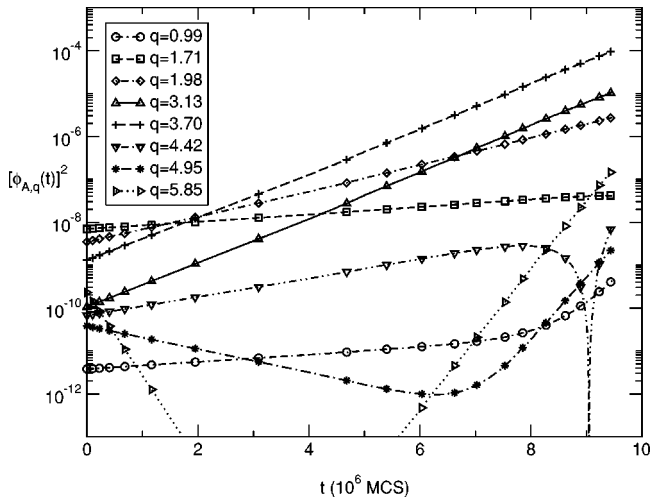

FIG. 2. Several density modes displayed on a logarithmic scale versus time. The displayed values of q are given in units of $1/R_e$. The results were obtained through DSCFT calculations in a three-dimensional system of length $L_x=L_y=L_z=6.35R_e$ using $7\times7\times7$ functions for a quench from $\chi N=0.314$ to $\chi N=5$. The expected exponential behavior during early stages of demixing is well reproduced.

IV. RESULTS

In the following sections we regard the early stages of spinodal decomposition after a quench from the one phase region with $\chi N=0.314$ into the miscibility gap with $\chi N=5$ for a symmetric binary polymer mixture. For much larger incompatibility the width of the interface becomes of the order of the statistical segment length, and properties on this length scale cannot be described by the Gaussian chain model. For smaller incompatibilities—in the vicinity of the critical point $\chi N=2$—composition fluctuations are very strong (i.e., non-Gaussian) and the mean field approximation becomes worse. We will first show some general results for the dynamical mean field theory. We will then carry on to compare these results with Monte Carlo simulations showing what role the Onsager coefficient plays. After having neglected random statistical fluctuations in SCFT so far we will explain how fluctuations are implemented into the two dynamic mean field theories and discuss their influence on the dynamics.

A. General aspects of spinodal decomposition

If a system is quenched from the one phase region into the two phase region the linearized theory of spinodal decomposition [9–11] predicts that fluctuations with wavelengths λ larger than a critical value λ_c, i.e., wave vectors q below a critical value q_c, start growing spontaneously. This is illustrated in Fig. 1 showing results obtained through DSCFT with local coupling in a one-dimensional system. Before the quench at time $t=0$ we have a homogeneous mixture with random statistical density fluctuations. After the quench these fluctuations are amplified. It is apparent that the resulting density profile is well describable with plane waves, so that the set of basis functions we have chosen proves to be not only technically convenient for the calculations but also describes the physical phenomena well. At later times we see that the mode with the wavelength about one-third of the system size is amplified most until at even later stages a saturation inside domains takes place until these domains are separated by sharp interfaces. Later stages of demixing are not appropriately described within our purely diffusive model because hydrodynamic mechanisms and random fluctuations are neglected but play a dominant role.

Linearized Cahn-Hilliard-Cook theory [9–11] predicts an exponential behavior for the density modes $\phi_A(\mathbf{q})\sim e^{R(q)t}$ as long as the difference $\phi_A(\mathbf{r})-\overline{\phi_A}$ between the actual density and the average density is small. Starting with a homogeneous mixture before the quench this requirement is fulfilled during early demixing. Our density coefficients $\phi_A(\mathbf{q})$ are equivalent to the actual, but discretized, density modes. In Fig. 2 some of the coefficients $\phi_A(\mathbf{q})$ are displayed versus time. These results were obtained for a three-dimensional system using DSCFT with a local Onsager coefficient. The exponential behavior is obviously well reproduced for early times. For larger values of q the exponential behavior changes earlier. This is also in agreement with experimental results [54]. The faster growth of density modes with smaller wave vectors leads to the creation of small domains on a length scale $\sim 1/q$. These domains then cause density modes with wavelengths smaller than the extension of the domain to be damped. Fig. 3 shows the corresponding relaxation rate $R(q)$ versus q. We see that for wave vectors with a value below q_c an exponential growth of the density modes sets in

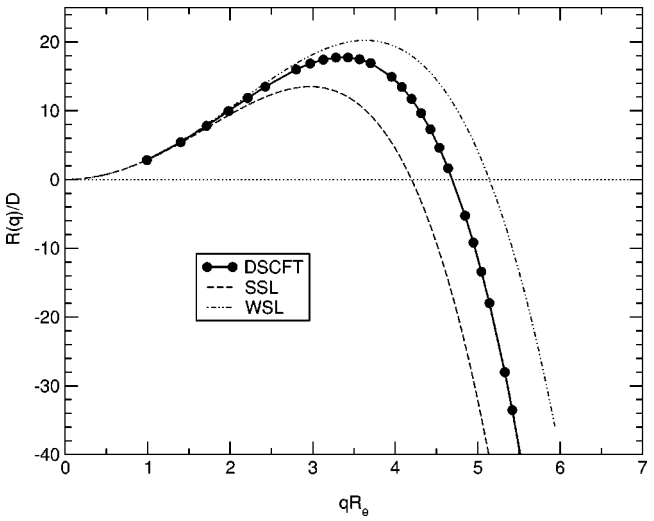

FIG. 3. Corresponding relaxation rate to the density modes displayed in Fig. 2. Below a critical wave vector q_c the density modes are increased spontaneously. Modes with larger wave vectors are damped. As expected the results are found to be between the two limits of weak (WSL) and strong segregation (SSL) as given by the Cahn-Hilliard-Cook theory.

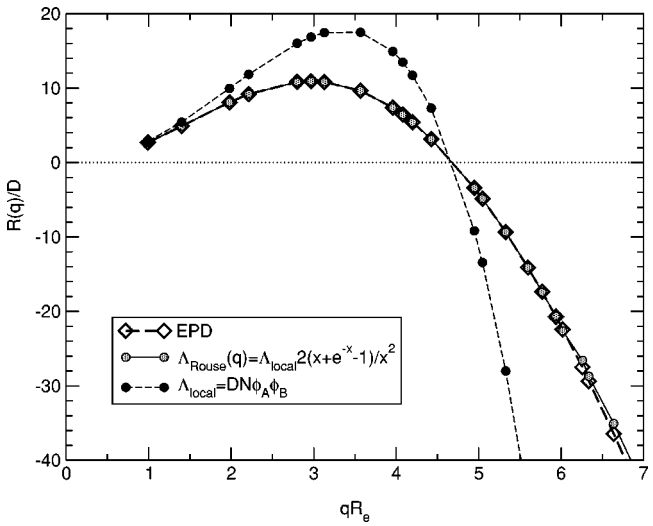

FIG. 4. Relaxation rates obtained through two-dimensional DSCFT calculations using local and Rouse dynamics and EPD calculations. The DSCFT results using the pair-correlation function of a homogeneous melt and the EPD results are in good agreement.

whereas for $q>q_c$ initial fluctuations are damped. In the growth region there is a maximum. The two dashed lines framing our results are the relaxation rates for temperatures just below the critical temperature (weak segregation limit, WSL) and for very low temperatures (strong segregation limit, SSL) as they are given by the Cahn-Hilliard-Cook theory,

$$\frac{R(q)}{q^2}=-2\Lambda(0)[\chi_S(\bar{\phi}_A)-\chi]\left(1-\frac{q^2}{q_c^2}\right), \tag{46}$$

with

$$q_c=\frac{\sqrt{2k}}{R_e}\sqrt{\bar{\phi}_A(1-\bar{\phi}_A)}[\chi N-\chi_S(\bar{\phi}_A)N]^{1/2}$$

$$=\frac{\sqrt{k}}{R_e}(\chi N/2-1)^{1/2}. \tag{47}$$

The last line is only valid for symmetric mixtures with $\bar{\phi}_A=\bar{\phi}_B=0.5$ when the spinodal point lies at $\chi_S N=2$. k is found to be 18 in the WSL [23] and 12 in the SSL [55]. The maximum growth rate is found for $q_m=q_c/\sqrt{2}$. With $\chi N=5$ lying between the SSL and the WSL our result was to be expected. The influence of Rouse dynamics on the relaxation rate is displayed in Fig. 4. Here we have presented results for a two-dimensional system using DSCFT with Onsager coefficients describing both local kinetics and Rouse kinetics for an approximately homogeneous mixture and EPD. The EPD and the DSCFT results using Rouse dynamics are virtually identical, but remembering that the EPD method is computationally much more favorable, this method should be used when Rouse kinetics is considered. Local and nonlocal couplings lead to distinct differences in the relaxation rates: in the range $0\leqslant q\leqslant q_c$ nonlocal coupling leads to a reduction of the relaxation rate and a shift of the maximum to smaller values of the wave vector. Also in the region $q>q_c$ the initial density fluctuations are not as strongly damped as for local dynamics.

Note that the difference in growth rate between the local dynamics in the WSL and SSL is very similar in magnitude to the difference in growth rate between the full SCFT calculation using a local or a Rouse-Onsager coefficient. This demonstrates that the square gradient expression for the free energy is not sufficiently accurate: quantitative deviations from experiments or simulations might be either due to the additional approximations of the square gradient approach or the wave vector dependence of the Onsager coefficient. To compare simulations and theory quantitatively and to extract the interplay between single chain dynamics and the kinetics of collective composition fluctuations, a quantitative self-consistent-field calculation is required.

B. Comparison between Monte Carlo results and dynamic mean field results

The Monte Carlo simulations were performed on a Cray T3E using a trivial parallelization scheme running 64 configurations in parallel to achieve good statistics. 5 400 000 MCS were performed that is equivalent to 45 days of CPU time per processor. The EPD and DSCFT calculations, the results of which are presented in this section, are for a three-dimensional system using $7\times7\times7=343$ basis functions. The equivalent of 12 700 000 MCS were performed taking approximately 65 days on a Cray J90.

The global structure factor defined by

$$S(q,t)=\left\langle \int_V d^3\mathbf{r}\{\phi_A(\mathbf{r},t)-\phi_B(\mathbf{r},t)\}^2 e^{i\mathbf{q}\cdot\mathbf{r}}\right\rangle, \tag{48}$$

is an important experimentally measurable quantity for the description of the phase separation process. In Fig. 5 the

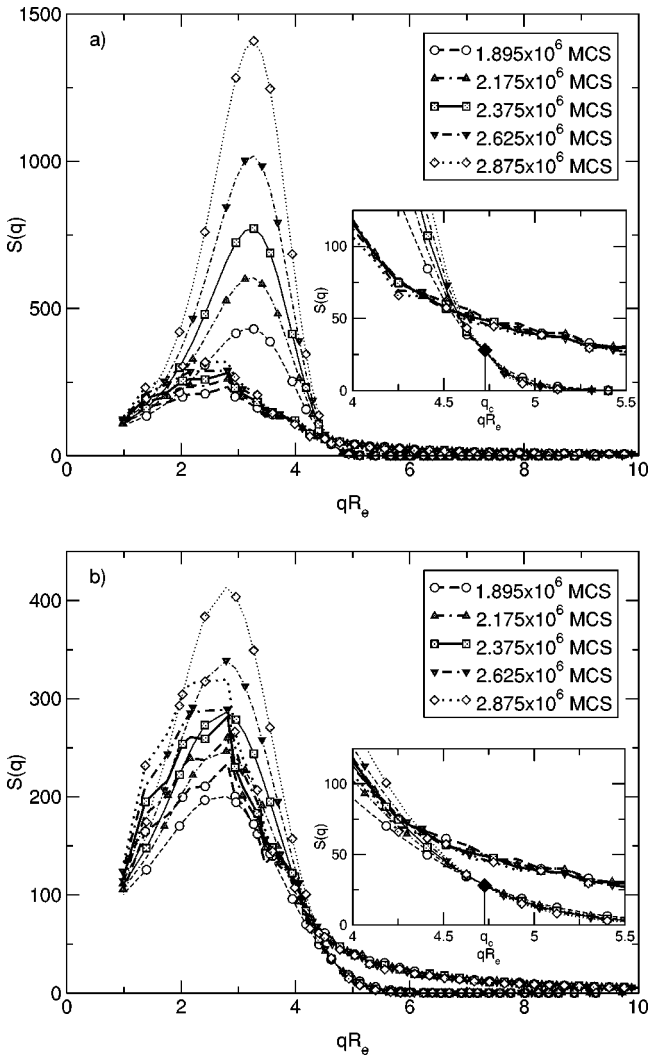

FIG. 5. Global structure factor versus wave vector for different times. Broader lines represent Monte Carlo results, thin lines with the same symbols the corresponding DSCFT results. Panel (a) compares DSCFT with local coupling with the Monte Carlo simulations. Local dynamics obviously overestimates the growth rate and shifts the maximum growth rate to larger values. Panel (b) compares Rouses dynamics with Monte Carlo results showing better agreement. The inset graphs show the behavior of the global structure factor in the area of q_c. While the mean field results lead to a common intersection point defining q_c, the Monte Carlo lines do not cross each other in a single point making the definition of q_c impossible.

global structure factor is plotted versus wave vector q for different times, thin lines denoting SCFT results, wide lines with the same symbols corresponding Monte Carlo simulation results. (Because the SCFT calculations could only be performed for a single starting configuration instead of 64 like in the Monte Carlo simulations, for the initial time, the global structure factor of a homogeneous mixture given by RPA [42] was used. Global structure factors for later times were extracted through the exponential time dependence of the density modes in the SCFT calculations.) Part (a) compares Monte Carlo with local kinetics and part (b) compares Monte Carlo with Rouse kinetics. Figure 5(a) clearly shows

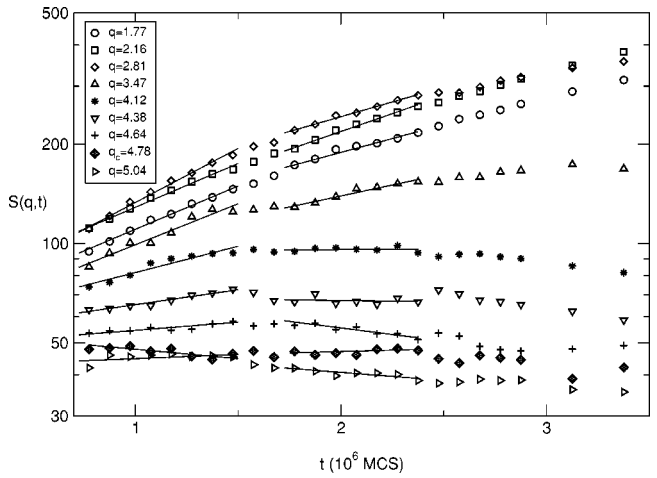

FIG. 6. Global structure factor versus time for a few randomly chosen values of q. The values of the wave vectors are given in units of $1/R_e$. q_c corresponds to the critical wave vector extracted from DSCFT. An exponential growth of the modes is found. Modes with a smaller growth rate change their exponential behavior earlier than those growing faster.

no quantitative agreement between DSCFT with local kinetics and the Monte Carlo simulations. The peak in SCFT grows much quicker and also the position of the peak is too far right. As has been mentioned before, including Rouse dynamics leads to a reduction of the relaxation rate in the growth region and the wave vector with the maximum growth rate is shifted towards a smaller value. Figure 5(b) satisfies these expectations. The position of the peaks for SCFT and Monte Carlo almost coincide and the growth rates of the peak are much closer to each other although SCFT still overestimates the growth rate. A more detailed comparison is possible if we plot the corresponding relaxation rates versus the wave vector. As we have seen before, the modes of the density calculated with the dynamic mean field theory follow a clear exponential behavior. To derive the relaxation rates of the global structure factor, we need to plot the modes of the global structure factor on a logarithmic scale versus time. This is done in Fig. 6 for some randomly chosen values of q. The modes with a q value smaller than the critical value q_c derived through DSCFT show a clear exponential behavior. This behavior changes with time, especially, the bigger the value of q of the growing mode, the sooner the change in the exponential behavior takes place. This is qualitatively in agreement with the results we obtained through dynamic mean field theory, see Sec. IV A. Modes with $q \gtrsim q_c$ are more or less constant in our figure. Therefore an estimation of q_c from the Monte Carlo results alone would suffer from some ambiguity, of course, this is not only because the accuracy of the Monte Carlo results is limited, but is a matter of principle [8]. The interplay of fluctuations and nonlinear effects has the consequence that a well-defined q_c does not exist. For times earlier than the displayed interval, random fluctuations influence the behavior of the modes so strongly that an exponential behavior is not visible. The relaxation rates resulting from the fits to the points in Fig. 6 for the two different time intervals indicated through the solid lines and

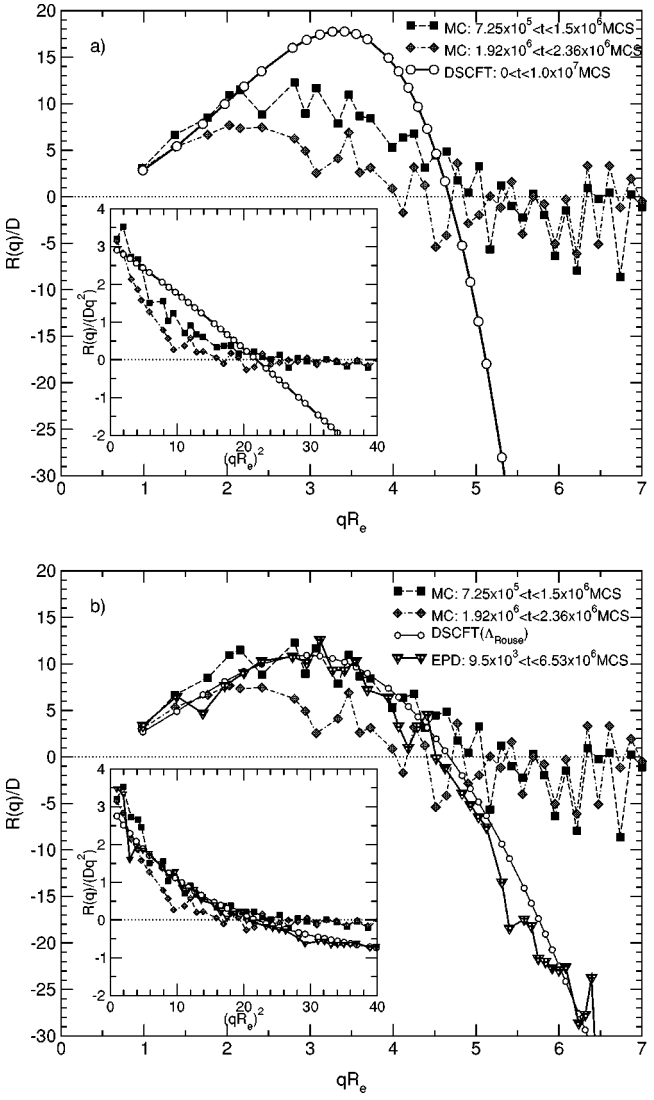

FIG. 7. Corresponding relaxation rates to Fig. 5. Panel (a) compares the Monte Carlo relaxation rates with DSCFT calculations with local dynamics. Panel (b) compares Monte Carlo results with EPD and DSCFT calculations with Rouse dynamics. For earlier times good agreement in the growth region is found but Monte Carlo simulations show an earlier change in the exponential behavior. The inset figures are the corresponding Cahn plots, where one displays $R(q)/q^2$ versus q^2.

the corresponding mean field relaxation rates are displayed in Fig. 7. Only the exponential behavior of the earlier of the two marked time intervals may be interpreted as the expected behavior of early spinodal decomposition. For later times a gradual change away from the exponential behavior sets in. The second fit shows an apparent exponential behavior because the time interval is too small to resolve the change. Hence the resulting ''relaxation rate'' for the later time interval may only be treated as an indication for the deviation from the earlier exponential behavior. Part (a) shows the relaxation rate for DSCFT with local dynamics in the time interval $0 \leqslant t \leqslant 1\times10^7$ MCS and the Monte Carlo results for the two time intervals $7.25\times10^5 \leqslant t \leqslant 1.5\times10^6$ MCS and $1.92\times10^6 \leqslant t \leqslant 2.63\times10^6$ MCS; part (b) shows the same results but regarding Rouse dynamics through the use of EPD and DSCFT with Rouse dynamics. The inset figures are the corresponding Cahn plots displaying $R(q)/q^2$ versus q^2. As is obvious from the behavior of the global structure factor, local dynamics gives a relaxation rate that is much too large and the wave vector of the maximal growth rate is also too big. The Cahn plot of the mean field relaxation rate shows the linear behavior, which is expected for local coupling. This is in strong disagreement with the Monte Carlo results. For Rouse dynamics we actually find an almost quantitative agreement for earlier times in the region of the positive growth rate. For later times, however, the relaxation rate decreases in the Monte Carlo simulations—this has also been observed in experimental studies [27]—, while SCFT still shows the same exponential behavior as is found for earlier times. In the Cahn plot we see that Rouse dynamics leads to a nonlinear run of $R(q)/q^2$ versus q^2. This is obviously also the case for the simulation results and is in agreement with earlier simulations [15–17] and experimental observations [27–29]. This nonlinear behavior of the Cahn plot is related to the fact that we consider a deep quench, for which $q_c R_e > 1$ [22]. For a shallow quench, for which χN exceeds the critical value $\chi_c N = 2$ [42] only slightly, one has $q_c R_e < 1$ [22], and then the theory would yield a linear Cahn plot, also consistent with corresponding observations [8]. The latter case is less interesting, however, because then the polymer mixture is to a large extent equivalent in behavior to a fluid mixture of small molecules, and there is no longer an effect of internal Rouse relaxation modes on the phase separation dynamics in this limit.

If we now compare our results for larger wave vectors we see big discrepancies independent of the chosen dynamics in SCFT: At q_c the structure factor is independent of time in the early stages of the SCFT calculations, i.e., structure factors at different times exhibit a common crossing point at q_c, see the inset graphs of Fig. 5. No such intersection occurs in the simulation data. Mean field theory damps the density modes with $q > q_c$ while Monte Carlo simulations lead to a relaxation rate fluctuating around zero. This behavior is also seen in the global structure factor, see Fig. 5. The right side of the SCFT peak decays fast, while the Monte Carlo peak is much broader with a slower decay. Both the earlier change of the exponential behavior and the form of the relaxation rate for larger wave vectors are the result of random fluctuations. As was expected, the influence of fluctuations during the very early stages of spinodal decomposition on the growth of the density modes is rather small, but they are crucial for smaller wavelengths and determine the change in the exponential behavior, because random fluctuations cause some modes to reach an amplitude where the nonlinear regime sets in early.

C. The influence of random fluctuations

The diffusion equations we have used so far are completely deterministic, but obviously in all dynamic processes random statistical fluctuations are present. To regard these fluctuations we have to add a random force η to our diffusion equations (19) and (40) that is linked to the Onsager coefficient through the fluctuation-dissipation theorem,

$$\langle \eta(\mathbf{r}) \rangle = 0,$$

$$\langle \eta(\mathbf{r},t)\, \eta(\mathbf{r}',t') \rangle = 2k_B T \Lambda(\mathbf{r},\mathbf{r}') \nabla^2 \delta(\mathbf{r}-\mathbf{r}')\, \delta(t-t'), \tag{49}$$

or Fourier transformed,

$$\langle \eta_q \rangle = 0,$$

$$\langle \eta_q(t)\, \eta_{-q}(t') \rangle = \langle |\eta_q|^2 \rangle = 2k_B T \Lambda(q) q^2 \delta(t-t'). \tag{50}$$

In our calculations the diffusion equation is integrated through discrete time intervals δt that are determined through the Runge-Kutta scheme. In DSCFT, for example, we use the Langevin equation

$$\phi_{A,q}(t+\delta t) = \phi_{A,q}(t) + \delta t \Lambda(q) q^2 \mu_q + f_q(\delta t), \tag{51}$$

with $f_q(\delta t)$ expressing random fluctuations that obey the fluctuation-dissipation theorem [56,57],

$$f_q(\delta t) = \sqrt{2\Lambda(q) q^2} \sqrt{\delta t}\ \ r, \tag{52}$$

r is a random number with the properties $\langle r \rangle = 0$, $\langle r^2 \rangle = 1$.

The analog $f_q(\delta t)$ is used to perform EPD calculations with fluctuations. The difficulty in this case is to interpret the resulting fluctuations of the external field $W = W_A - W_B$ in terms of the density $\Phi = (\phi_A - \phi_B)/2$. As we have seen in Sec. II C the field and the density fluctuations are linked to each other through Eqs. (38) and (39).

To ensure that the way the fluctuations are included is correct and the validity of these Eqs. (38) and (39) is given, we consider a homogeneous, $\chi N = 1.8$, one-dimensional system with length $L_x = 6.35 R_e$ using both DSCFT and EPD. From the DSCFT calculations we derive $\langle |\Phi_q|^2 \rangle$ for each wave vector while the EPD method leads to $\langle |W_q|^2 \rangle$. In both cases we averaged over 10 000 snapshots of the density or the field made during their time evolution. In Fig. 8 $\langle |\Phi_q|^2 \rangle$ and $\langle |W_q|^2 \rangle$ are plotted versus q. The solid line is the expected result from RPA. For larger values of q we find good agreement, but the amount of used configurations was not enough to find reliable results for smaller values of q because the correlation times are much longer due to the diffusive dynamics. If we plot $\langle |\Phi_q|^2 \rangle$ versus $\langle |W_q|^2 \rangle$, as is done in Fig. 9, we find good agreement of our data with the expected linear behavior.

After having proven that the above treatment of random fluctuations leads to the expected behavior, we focus on the influence of fluctuations on spinodal decomposition. Monte Carlo results show that the exponential behavior changes earlier than in SCFT calculations without fluctuations resulting in a reduced relaxation rate. The relaxation rates for different time intervals obtained through the Monte Carlo simulations and the EPD method are presented in Fig. 10. The EPD results were obtained by averaging the time evolution of the fields of 64 two-dimensional configurations. For earlier time intervals the relaxation rate is quantitatively very similar to the rate without fluctuations in the region below q_c. For later times, however, when calculations without fluctuations still show the same exponential behavior, the relaxation rate is reduced as is also seen in the Monte Carlo simulations. In the range above q_c the modes of the fields or densities do not follow an exponential behavior but fluctuate around zero. Consequently the relaxation rate is not well defined in this region leading to strong fluctuations of the relaxation rate in Fig. 10. For very early times when the density modes are still of the order of the fluctuations of the homogeneous system it is also not possible to see an exponential behavior because the density changes caused through random fluctuations conceal the growth of the modes during very early spinodal decomposition.

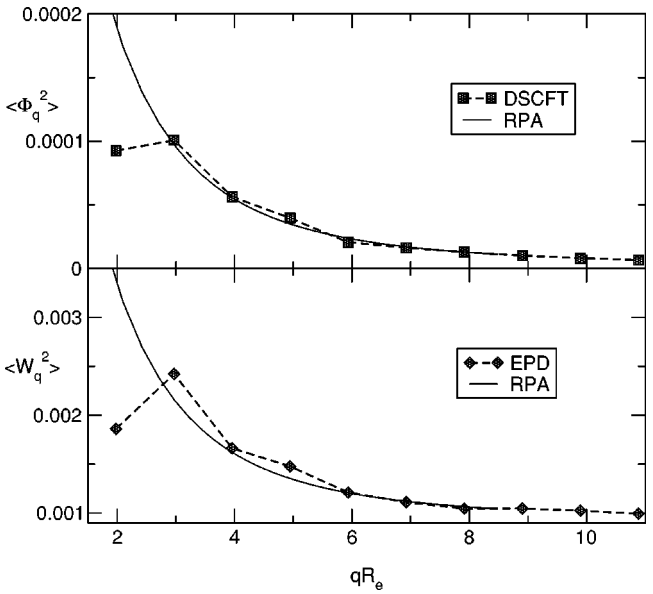

FIG. 8. The average $\langle |\Phi_q|^2 \rangle$ derived with DSCFT and $\langle |W_q|^2 \rangle$ derived with EPD displayed versus q. Both calculations are valid for a homogeneous, $\chi N = 1.8$, one-dimensional system with length $L = 6.35 R_e$. For larger values of q good agreement with the RPA averages is found. For smaller values of q too few independent configurations of the system were taken into account.

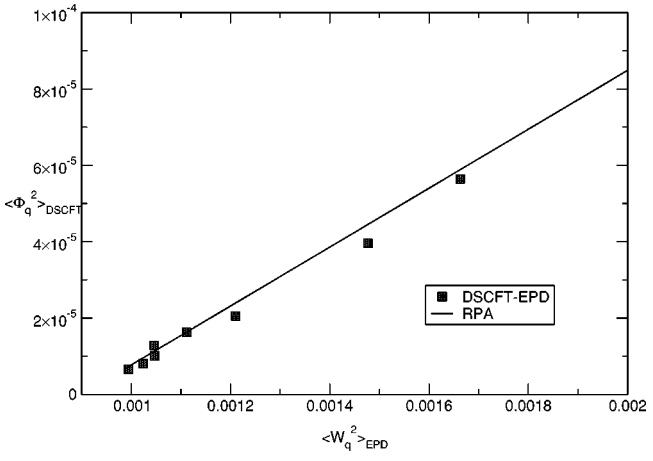

FIG. 9. The linear behavior expressed in Eq. (39) is well reproduced, as we can see, when $\langle |\Phi_q|^2 \rangle$, obtained through DSCFT, is displayed versus $\langle |W_q|^2 \rangle$, obtained through EPD. The points to the right correspond to small wave vectors, those on the left to large wave vectors. The solid line is the corresponding RPA result.

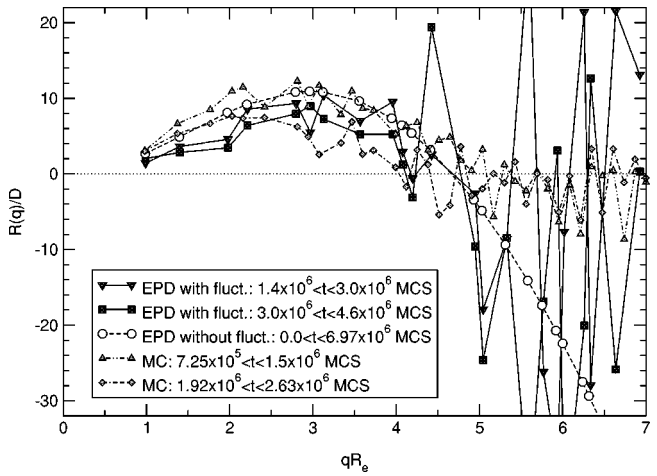

FIG. 10. Relaxation rates obtained through Monte Carlo simulations and EPD calculations in two dimensions with random fluctuations for different time intervals. Fluctuations lead in both methods to an earlier change in the exponential behavior of the increasing modes.

V. SUMMARY

In this study we analyzed the influence of single chain dynamics on the collective diffusion during early stages of spinodal decomposition in a symmetric binary polymer blend. We used the SCFT for polymer mixtures to explore two versions of dynamical mean field theory. The single chain dynamics enters these descriptions through an Onsager coefficient. The first method we call DSCFT propagates the densities in time and gives us the possibility to model both local dynamics and approximately the nonlocal dynamics we expect for the Rouse model. In DSCFT the correct treatment of Rouse dynamics would involve the calculation of the pair-correlation function at every time step, which is computationally a rather expensive task. On the other hand during early stages of demixing, the mixture is only weakly inhomogeneous so that the use of the pair-correlation function of a homogeneous mixture, which is analytically known, serves as a sufficient approximation. In the second method the instantaneous configuration is not described by the densities but by the effective external field (EPD). We find a Langevin equation for the external field, which using ''local'' kinetics in the fields is found to describe a polymer mixture with Rouse dynamics. Apart from ''automatically'' including Rouse dynamics, this EPD method has the big advantage of being up to an order of magnitude computationally faster than the DSCFT method.

First numerical calculations with these methods for a quench from the one phase region $\chi N=0.314$ to the two phase region $\chi N=5$, neglecting random fluctuations, show a clear exponential behavior of the density modes, as was expected for a mean field description. The relaxation rate of the density mode is strongly influenced by the choice of the Onsager coefficient: In the growth region Rouse dynamics reduces the relaxation rate compared to local dynamics and the position of the maximum growth rate is shifted to smaller values of q. For $q>q_c$, however, Rouse dynamics causes the modes to be damped less quickly. We also find good agreement for early stages between the DSCFT method using the pair-correlation function for the homogeneous system and the EPD method.

To quantitatively test these mean field predictions we compare them with results obtained through Monte Carlo simulations employing the bond fluctuation model. The chains used in these simulations are expected to show Rouse behavior because of the chosen chain length $N=64$. The comparison is possible without any adjustable parameter. We compare the global structure factor, which is the experimentally accessible quantity, and the relaxation rates. Local dynamics in DSCFT overestimates the growth of the global structure factor by far, but the agreement is better for Rouse dynamics especially for earlier times. Neglecting random fluctuations in our mean field calculations proves to be justified for wave vectors with positive relaxation rates and earlier times, but should be included to investigate later times.

Fluctuations can easily be included in DSCFT and EPD. The difficulty in the EPD method is the fact that the field fluctuations have to be interpreted in terms of the physical density fluctuations. We can find a relation between the field and the density fluctuations. EPD calculations with fluctuations lead to an earlier change in the exponential behavior of the density modes as was also the case for the Monte Carlo simulations. The missing dampening of the modes with $q>q_c$ as is found in the simulations is also reproduced.

We have seen that the single chain dynamics has a pronounced influence on the collective dynamics of a polymer mixture. Comparing quantitatively Monte Carlo simulations and dynamical mean field theory we have validated the mean field calculations. Note, however, that we have considered a deep quench far below the critical point; for shallow quenches close to the critical point, mean field theories are not expected to be accurate. The later stages of spinodal decomposition are not accessible with either method. During later times hydrodynamical interactions become important. Lattice model Monte Carlo simulations lack a hydrodynamical mechanism. In dynamical mean field calculations hydrodynamic coupling can be included [58,59], and hence, they can be extended beyond the validity of the lattice model.

ACKNOWLEDGMENTS

We have benefitted from discussion with D. Düchs, F. Schmid, and V. Ganesan. Financial support was provided by the Graduierten Kolleg ''supramolecular systems'' of the University of Mainz and the DFG under Grant No. Bi314/17 in the priority program ''wetting and structure formation at interfaces.'' Generous access to computers at the NIC Jülich and the HLR Stuttgart are gratefully acknowledged.

APPENDIX A: REPRESENTATION OF ROUSE DYNAMICS THROUGH EPD

As mentioned before it is possible to show that the EPD method using local coupling is a good approximation for reproducing Rouse dynamics of the physical densities. The derivation of the EPD method we present in this section was

introduced by Maurits and Fraaije and can be found in Ref. [26].

Following the method we used to include dynamics in the SCFT to achieve the DSCFT method, we employ a saddle point approximation in the external fields that leads to a bijective relation between the external fields w_A and w_B and the densities ϕ_A and ϕ_B. This means we can choose with which of the two variable sets we would like to calculate. On the other hand the pair-correlation function that is part of the Rouse-Onsager coefficient can be expressed as the functional derivative of the density with respect to the external potential, see also Eq. (B13).

$$\frac{\delta\phi_A(\mathbf{r})}{\delta w_A(\mathbf{r}')} = -\frac{\overline{\phi}_A}{N} P_0(\mathbf{r},\mathbf{r}'). \tag{A1}$$

To calculate in w space we have to transform the time derivative of the densities according to the chain rule

$$\begin{aligned}\frac{\partial\phi_A(\mathbf{r},t)}{\partial t} &= \int \frac{\delta\phi_A(\mathbf{r},t)}{\delta w_A(\mathbf{r}',t)} \frac{\partial w_A(\mathbf{r}',t)}{\partial t} d\mathbf{r}'^3 \\ &= -\frac{\overline{\phi}_A}{N} \int P_0(\mathbf{r},\mathbf{r}') \frac{\partial w_A(\mathbf{r}',t)}{\partial t} d\mathbf{r}'^3. \end{aligned} \tag{A2}$$

Combining this equation with the diffusion equation for Rouse dynamics, Eq. (18), this leads us to

$$\begin{aligned} -\frac{\overline{\phi}_A}{N} \int P_0(\mathbf{r},\mathbf{r}') \frac{\partial w_A(\mathbf{r}',t)}{\partial t} d\mathbf{r}'^3 \\ = D\frac{\overline{\phi}_A}{N} \nabla_{\mathbf{r}} \cdot \int_V P_0(\mathbf{r},\mathbf{r}') \nabla_{\mathbf{r}'} \mu_A(\mathbf{r}') d\mathbf{r}'^3. \end{aligned} \tag{A3}$$

Using the approximation

$$\nabla_{\mathbf{r}} P_0(\mathbf{r},\mathbf{r}') \cong -\nabla_{\mathbf{r}'} P_0(\mathbf{r},\mathbf{r}'), \tag{A4}$$

one easily arrives at

$$\begin{aligned} -\int_V P_0(\mathbf{r},\mathbf{r}') \frac{\partial w_A(\mathbf{r}',t)}{\partial t} d\mathbf{r}'^3 \\ = D\int_V P_0(\mathbf{r},\mathbf{r}') \nabla^2_{\mathbf{r}'} \mu_A(\mathbf{r}') d\mathbf{r}'^3, \end{aligned} \tag{A5}$$

leading to an equation of motion for the external fields,

$$\frac{\partial w_A(\mathbf{r})}{\partial t} = -D\nabla^2 \mu_A(\mathbf{r}). \tag{A6}$$

Approximation (A4) is obviously exactly valid for a homogeneous mixture, because the pair-correlation function only depends on the distance $|\mathbf{r}-\mathbf{r}'|$ between two points. In the inhomogeneous case, if $\mathbf{r}$ and $\mathbf{r}'$ are in different phases and neither of them in the interface, $\nabla_{\mathbf{r}} P_0(\mathbf{r},\mathbf{r}')$ and $\nabla_{\mathbf{r}'} P_0(\mathbf{r},\mathbf{r}')$ are of different sign making this approximation justifiable even if the actual values differ.

Because of the incompressibility constraint μ_A and μ_B are not independent of each other. There is only one independent chemical potential $\mu = \mu_A - \mu_B$ so the equation of motion for the external fields that is to be used in our case has the form:

$$\frac{\partial w_A(\mathbf{r})}{\partial t} - \frac{\partial w_B(\mathbf{r})}{\partial t} = -D\nabla^2 \mu(\mathbf{r}). \tag{A7}$$

If we compare this equation with Eq. (40) we see that densities evolving in time according to Rouse dynamics are well described through the EPD method if a local kinetic coefficient as given in Eq. (43) is used.

APPENDIX B: RANDOM PHASE APPROXIMATION FOR THE FLUCTUATIONS IN EPD

The single chain partition function Q is defined through [compare with Eq. (6)]

$$Q = \int \mathcal{D}[\mathbf{r}_1] \mathcal{P}_1[\mathbf{r}] \exp\left[-\frac{\rho}{N} \int_V d^3\mathbf{r} \;\; W(\mathbf{r}) \hat{\phi}_1(\mathbf{r}) \right], \tag{B1}$$

where $\hat{\phi}_1(\mathbf{r}) = (N/\rho)\int ds \;\; \delta(\mathbf{r}-\mathbf{r}(s))$ denotes the single chain density. We now expect the system to be only weakly inhomogeneous, i.e., meaning the density and the external field only differ a little from the average value: $\hat{\phi}_1(\mathbf{r}) = N/\rho V + \delta\phi_1(\mathbf{r})$; $W(\mathbf{r}) = \overline{W} + \delta W(\mathbf{r})$. The density and the external field are presented as a Fourier expansion,

$$\hat{\phi}_1(\mathbf{r}) = N/\rho V + \sum_{\mathbf{q}\neq 0} \hat{\phi}_{\mathbf{q}} e^{i\mathbf{q}\cdot\mathbf{r}}, \quad \hat{\phi}_{\mathbf{q}} = \frac{1}{V}\int_V d^3\mathbf{r} \;\; \hat{\phi}_1(\mathbf{r}) e^{-i\mathbf{q}\cdot\mathbf{r}}. \tag{B2}$$

This Fourier expansion is now inserted in Eq. (B1),

$$\begin{aligned} Q &= \int \mathcal{D}[\mathbf{r}_1] \mathcal{P}_1[\mathbf{r}] \exp\left[-\overline{W} - \frac{\rho V}{N} \sum_{\mathbf{q}\neq 0} W_{\mathbf{q}} \hat{\phi}_{-\mathbf{q}} \right] \\ &= \exp[-\overline{W}] \int \mathcal{D}[\mathbf{r}_1] \mathcal{P}_1[\mathbf{r}_1] \left\{ 1 - \frac{\rho V}{N} \sum_{\mathbf{q}\neq 0} W_{\mathbf{q}} \hat{\phi}_{-\mathbf{q}} \right. \\ &\quad \left. + \frac{\rho^2 V^2}{2N^2} \sum_{\mathbf{q},\mathbf{q}'\neq 0} W_{\mathbf{q}} W_{\mathbf{q}'} \hat{\phi}_{-\mathbf{q}} \hat{\phi}_{-\mathbf{q}'} + \cdots \right\} \\ &= \exp[-\overline{W}] Q_0 \left\langle 1 - \frac{\rho V}{N} \sum_{\mathbf{q}\neq 0} W_{\mathbf{q}} \hat{\phi}_{-\mathbf{q}} \right. \\ &\quad \left. + \frac{\rho^2 V^2}{2N^2} \sum_{\mathbf{q},\mathbf{q}'\neq 0} W_{\mathbf{q}} W_{\mathbf{q}'} \hat{\phi}_{-\mathbf{q}} \hat{\phi}_{-\mathbf{q}'} + \cdots \right\rangle_0. \end{aligned} \tag{B3}$$

Q_0 denotes the partition function of a single chain without an external field. The average in the last line is to be taken over all chain configurations that are possible when there is no external field present. Because the average deviation of the density $\langle \delta\phi \rangle_0$ from the average value is zero if there is no external field, $\langle \phi_{\mathbf{q}} \rangle_0 = 0$ is valid. The average $\langle \phi_{-\mathbf{q}} \phi_{-\mathbf{q}'} \rangle_0$ is

given through the single chain structure factor $S_0(\mathbf{q})$ of a Gaussian chain: $\langle \phi_{-\mathbf{q}} \phi_{-\mathbf{q}'} \rangle_0 = N/(\rho^2 V^2) S_0(\mathbf{q}) \delta_{-\mathbf{q},-\mathbf{q}'}$. Neglecting higher terms, we obtain the RPA result for the single chain partition function

$$Q^{\mathrm{RPA}} = \exp[-\overline{W}] Q_0 \exp\left[\frac{1}{2N} \sum_{\mathbf{q}\neq 0} S_0(\mathbf{q}) |W_{\mathbf{q}}|^2 \right]. \quad \text{(B4)}$$

Obviously a corresponding expression is valid for an A and B polymer. These RPA single chain partition functions are plugged into Eq. (26) leading to

$$\begin{aligned} \frac{G[U,W]}{k_B T} = & -\frac{\overline{\phi}_A \rho V}{N} \ln \frac{Q_{A,0}}{n_A} - \frac{\overline{\phi}_B \rho V}{N} \ln \frac{Q_{B,0}}{n_B} + \frac{\rho V \chi}{4} \\ & + \frac{(\overline{\phi}_A - \overline{\phi}_B) \rho V \overline{W}}{2N} + \frac{\rho V}{4N\chi N} \overline{W}^2 \\ & + \frac{\rho V}{4N\chi N} \sum_{\mathbf{q}\neq 0} |W_{\mathbf{q}}|^2 \\ & - \frac{\overline{\phi}_A \rho V}{2N^2} \sum_{\mathbf{q}\neq 0} S_0(\mathbf{q}) \left| \frac{(W_{\mathbf{q}} + U_{\mathbf{q}})}{2} \right|^2 \\ & - \frac{\overline{\phi}_B \rho V}{2N^2} \sum_{\mathbf{q}\neq 0} S_0(\mathbf{q}) \left| \frac{(U_{\mathbf{q}} - W_{\mathbf{q}})}{2} \right|^2. \end{aligned} \quad \text{(B5)}$$

Regarding only the wave vector dependent parts of the free energy we find

$$\begin{aligned} \frac{G[U,W]}{k_B T} = & -\frac{\rho V}{2N^2} \sum_{\mathbf{q}\neq 0} \left\{ \left[\frac{S_0(\mathbf{q})}{4} - \frac{1}{2\chi} \right] |W_{\mathbf{q}}|^2 \right. \\ & \left. + \left[\frac{S_0(\mathbf{q})}{4} \right] |U_{\mathbf{q}}|^2 \right\} - \frac{\rho V}{2N^2} \\ & \times \sum_{\mathbf{q}\neq 0} \left\{ \frac{\overline{\phi}_A - \overline{\phi}_B}{2} S_0(\mathbf{q}) (U_{\mathbf{q}} W_{-\mathbf{q}}) \right\} + G_{\mathrm{hom}} \\ = & -\frac{\rho V}{2N^2} \sum_{\mathbf{q}\neq 0} \left\{ \left[\frac{S_0(\mathbf{q})}{4} - \frac{1}{2\chi} \right. \right. \\ & \left. \left. - \frac{1}{4} (\overline{\phi}_A - \overline{\phi}_B)^2 S_0(\mathbf{q}) \right] |W_{\mathbf{q}}|^2 \right\} \\ & - \frac{\rho V}{2N^2} \sum_{\mathbf{q}\neq 0} \left\{ \frac{S_0(\mathbf{q})}{4} |U_{\mathbf{q}} + (\overline{\phi}_A - \overline{\phi}_B) W_{\mathbf{q}}|^2 \right\} \\ & + G_{\mathrm{hom}}. \end{aligned} \quad \text{(B6)}$$

We use this free energy to evaluate the partition function of Eq. (25). Following the procedure we used before, we employ a saddle point approximation with respect to the field U,

$$\left. \frac{\delta F[U,W]}{\delta U} \right|_{U^*} = 0, \quad U^*_{\mathbf{q}} = -(\overline{\phi}_A - \overline{\phi}_B) W_{\mathbf{q}}. \quad \text{(B7)}$$

Since the free energy is quadratic in the RPA approximation the saddle point integration is equivalent to the functional integration over U. This again leads us to an expression for the free energy $G[W]$ only depending on the external field variable W,

$$\frac{G[W]}{k_B T} = \frac{\rho V}{2N^2} \sum_{\mathbf{q}\neq 0} \left[\overline{\phi}_A \overline{\phi}_B S_0(\mathbf{q}) - \frac{1}{2\chi} \right] |W_{\mathbf{q}}|^2 + G_{\mathrm{hom}}. \quad \text{(B8)}$$

Now the average $\langle |W_{\mathbf{q}}|^2 \rangle$ can be calculated,

$$\langle |W_{\mathbf{q}}|^2 \rangle = \frac{N^2}{\rho V} \frac{2\chi}{1 - 2\chi \overline{\phi}_A \overline{\phi}_B S_0(\mathbf{q})}. \quad \text{(B9)}$$

Using our result (39)

$$\langle |\hat{\phi}_{A\mathbf{q}} - \hat{\phi}_{B\mathbf{q}}|^2 \rangle = -\frac{4}{\rho V \chi} + \frac{1}{(\chi N)^2} \langle |W_{\mathbf{q}}|^2 \rangle, \quad \text{(B10)}$$

we express the density fluctuations in terms of the field fluctuations and recover the well-known RPA expression [42],

$$\begin{aligned} \langle |\hat{\phi}_{A\mathbf{q}} - \hat{\phi}_{B\mathbf{q}}|^2 \rangle &= \frac{4}{\rho V} \left[\frac{1}{\overline{\phi}_A S_0(\mathbf{q})} + \frac{1}{\overline{\phi}_B S_0(\mathbf{q})} - 2\chi \right]^{-1} \\ &\equiv 4 S_{\mathrm{RPA}}(\mathbf{q}). \end{aligned} \quad \text{(B11)}$$

Using the RPA single chain partition function (B4), we calculate

$$\phi^*_A(\mathbf{r}) = -\frac{\overline{\phi}_A V}{Q_A} \frac{\delta Q_A}{\delta W_A(\mathbf{r})} = \overline{\phi}_A - \frac{\overline{\phi}_A}{N} \sum_{\mathbf{q}\neq 0} S_0(\mathbf{q}) W_{A\mathbf{q}} e^{i\mathbf{q}\cdot\mathbf{r}} \quad \text{(B12)}$$

$$\frac{\delta \phi^*_A(\mathbf{r})}{\delta W_A(\mathbf{r}')} = -\frac{\overline{\phi}_A}{NV} \sum_{\mathbf{q}\neq 0} S_0(\mathbf{q}) e^{i\mathbf{q}\cdot(\mathbf{r}-\mathbf{r}')}. \quad \text{(B13)}$$

The last equation is equivalent to Eq. (A1) but due to the particle conservation the $\mathbf{q}=0$ contribution has to be taken out of the sum. $\phi_A(\mathbf{q}=0)$ is just the average overall density $\overline{\phi}_A$ that cannot change if the external field is altered. With these expressions we obtain for the ''literal'' fluctuations in the EPD method according to Eq. (31),

$$\begin{aligned} & \langle |\hat{\phi}_{A\mathbf{q}} - \hat{\phi}_{B\mathbf{q}}|^2 \rangle_{\mathrm{EPD}} \\ & \quad = \langle |\phi^*_{A\mathbf{q}} - \phi^*_{B\mathbf{q}}|^2 \rangle \\ & \qquad - \frac{N}{\rho V^2} \int d^3\mathbf{r} \; d^3\mathbf{r}' \; e^{i\mathbf{q}\cdot(\mathbf{r}-\mathbf{r}')} \left\langle \frac{\delta \phi^*_A(\mathbf{r})}{\delta W_A(\mathbf{r}')} + \frac{\delta \phi^*_B(\mathbf{r})}{\delta W_B(\mathbf{r}')} \right\rangle \\ & \quad = \frac{8\chi S_0^2(\mathbf{q}) \overline{\phi}_A^2 \overline{\phi}_B^2}{\rho V [1 - 2\chi \overline{\phi}_A \overline{\phi}_B S_0(\mathbf{q})]} + \frac{S_0(\mathbf{q})}{\rho V} \\ & \quad = 4 S_{\mathrm{RPA}}(\mathbf{q}) + \frac{(1 - 4\overline{\phi}_A \overline{\phi}_B) S_0(\mathbf{q})}{\rho V}. \end{aligned} \quad \text{(B14)}$$

Generally, the deviation for the RPA result is of similar magnitude as the RPA structure factor itself. For a symmetric quench $\overline{\phi}_A = \frac{1}{2}$, however, we accidentally recover the RPA result. This example also illustrates that one can obtain the average of the composition by sampling the average of $\phi_A^* - \phi_B^*$, i.e., the densities of single chains in the field configuration W, but one should not use this to calculate fluctuations.

[1] D.R. Paul and S. Newman, *Polymer Blends*, 2nd ed. (Academic Press, San Diego, CA, 1978).
[2] M.J. Folbes and P.S. Hope, *Polymer Blends and Alloys*, 2nd ed. (Blackie Academic & Professional, London, 1993).
[3] E. Helfand and Y. Tagami, J. Chem. Phys. **56**, 3592 (1972).
[4] E. Helfand, J. Chem. Phys. **62**, 999 (1975).
[5] K.M. Hong and J. Noolandi, Macromolecules **14**, 727 (1981).
[6] M.W. Matsen and M. Schick, Phys. Rev. Lett. **72**, 2660 (1994).
[7] K.S. Schweizer and J.G. Curro, Adv. Chem. Phys. **97**, 1 (1997).
[8] For introductory reviews on spinodal decomposition, see K. Binder, in *Phase Transformations in Materials*, edited by P. Hansen (VCH, Weinheim, 1991), p. 405; T. Hashimoto, in *Structure and Properties of Polymers*, edited by E.J. Kramer (VCH, Weinheim, 1993), p. 251.
[9] J.W. Cahn and J.E. Hilliard, J. Chem. Phys. **28**, 258 (1958).
[10] J.W. Cahn and J.E. Hilliard, J. Chem. Phys. **31**, 668 (1959).
[11] H.E. Cook, Acta Metall. **18**, 297 (1970).
[12] M. Kotnis and M. Muthukumar, Macromolecules **25**, 1716 (1992).
[13] A. Chakrabarti, R. Toral, J.D. Gunton, and M. Muthukumar, Phys. Rev. Lett. **63**, 2072 (1989).
[14] C. Castellano and S.C. Glotzer, J. Chem. Phys. **103**, 9363 (1995).
[15] A. Sariban and K. Binder, Polym. Commun. **30**, 205 (1989).
[16] A. Sariban and K. Binder, Macromolecules **24**, 578 (1991).
[17] A. Baumgärtner and D.W. Heermann, Polymer **27**, 1777 (1986).
[18] J.G.E.M. Fraaije, J. Chem. Phys. **99**, 9202 (1993).
[19] J.G.E.M. Fraaije, B.A.C. van Vlimmeren, N.M. Maurits, M. Postma, O.A. Evers, C. Hoffmann, P. Altevogt, and G. Goldbeck-Wood, J. Chem. Phys. **106**, 4260 (1997).
[20] C. Yeung and A.C. Shi, Macromolecules **32**, 3637 (1999).
[21] R. Hasegawa and M. Doi, Macromolecules **30**, 3086 (1997).
[22] K. Binder, J. Chem. Phys. **79**, 6387 (1983).
[23] P.G. de Gennes, J. Chem. Phys. **72**, 4756 (1980).
[24] P. Pincus, J. Chem. Phys. **75**, 1996 (1981).
[25] B.A.C. van Vlimmeren, N.M. Maurits, A.V. Zvelindovsky, G.J.A. Sevink, and J.G.E.M. Fraaije, Macromolecules **32**, 646 (1999).
[26] N.M. Maurits and J.G.E.M. Fraaije, J. Chem. Phys. **107**, 5879 (1997).
[27] G. Müller, D. Schwahn, H. Eckerlebe, J. Rieger, and T. Springer, J. Chem. Phys. **104**, 5326 (1996).
[28] D. Schwahn, S. Janssen, and T. Springer, J. Chem. Phys. **97**, 8775 (1992).
[29] H. Jinnai, H. Hasegawa, T. Hashimoto, and C.C. Han, J. Chem. Phys. **99**, 8154 (1993).
[30] H.M. Tanaka, J. Phys.: Condens. Matter **12**, R207 (2000).
[31] H.M. Tanaka, Prog. Theor. Phys. **101**, 863 (1999).
[32] I. Carmesin and K. Kremer, J. Phys. (France) **51**, 915 (1990).
[33] H.P. Deutsch and K. Binder, J. Chem. Phys. **94**, 2294 (1991).
[34] M. Müller, Macromol. Theory Simul. **8**, 343 (1999).
[35] A. Werner, F. Schmid, M. Müller, and K. Binder, Phys. Rev. E **59**, 728 (1999).
[36] A.C. Shi, J. Noolandi, and R.C. Desai, Macromolecules **29**, 6487 (1996).
[37] This is a common practice in self-consistent-field calculations. It is understood that the incompressibility constraint is enforced only after coarse graining the microscopic densities over a small but finite volume. On smaller length scales the specific spatial dependence of the repulsive interactions matters and leads, e.g., to packing effects. This is beyond our treatment.
[38] P.E. Rouse, J. Chem. Phys. **21**, 1272 (1953).
[39] M. Doi and S.F. Edwards, *The Theory of Polymer Dynamics* (Oxford University Press, Oxford 1994).
[40] P.G. de Gennes, J. Chem. Phys. **55**, 572 (1971).
[41] J.E. Dennis, Jr. and R.B. Schnabel, *Numerical Methods for Unconstrained Optimization and Nonlinear Equations* (Prentice-Hall, Englewood Cliffs, NJ, 1983).
[42] P.-G. de Gennes, *Scaling Concepts in Polymer Physics* (Cornell University Press, Ithaca, 1979).
[43] V. Ganesan and G.H. Fredrickson, Europhys. Lett. (to be published).
[44] P.C. Hohenberg and B.I. Halperin, Rev. Mod. Phys. **49**, 435 (1977).
[45] W. Paul, K. Binder, D.W. Heermann, and K. Kremer, J. Chem. Phys. **95**, 7726 (1991).
[46] W. Paul, K. Binder, D.W. Heermann, and K. Kremer, J. Phys. II **1**, 37 (1991).
[47] M. Müller and K. Binder, Macromolecules **28**, 1825 (1995).
[48] M. Müller and K. Binder, J. Phys. II **6**, 187 (1996).
[49] T. Kreer, J. Baschnagel, M. Müller, and K. Binder, Macromolecules **34**, 1105 (2001).
[50] M. Müller, J.P. Wittmer, and J.L. Barrat, Europhys. Lett. **52**, 406 (2000).
[51] M. Müller, E.V. Albano, and K. Binder, Phys. Rev. E **62**, 5281 (2000).
[52] N. Saito, K. Takahashi, and Y. Yunoki, J. Phys. Soc. Jpn. **85**, 219 (1967).
[53] D.C. Morse and G.H. Fredrickson, Phys. Rev. Lett. **73**, 3235 (1994).
[54] H. Jinnai, H. Hasegawa, T. Hashimoto, and C.C. Han, J. Chem. Phys. **99**, 4845 (1993).
[55] R.J. Roe, Macromolecules **19**, 728 (1986).
[56] B.A.C van Vlimmeren and J.G.E.M. Fraaije, Comput. Phys. Commun. **99**, 21 (1996).
[57] C.W. Gardiner, *Handbook of Stochastic Methods*, 2nd ed. (Springer-Verlag, Berlin, 1990).
[58] N.M. Maurits, A.V. Zvelindovsky, and J.G.E.M. Fraaije, J. Chem. Phys. **108**, 9150 (1998).
[59] T. Koga, K. Kawasaki, M. Takenaka, and T. Hashimoto, Physica A **198**, 473 (1993).